ing a German-supplied version of the alpha proton–x-ray analyzer and a neutron detection device. The US is currently developing a soil oxidant detection experiment based upon chemical interaction of thin coatings on fiber optic cables, monitored for changes by reflection of light-emitting diode pulses. In 1996 a small instrumented rover will be sent, and the heavily instrumented French/Russian balloon will be launched.

Comets

For several years a group of composition analytical instruments have been under development for a comet rendezvous mission, specifically for the canceled 'CRAF' mission by NASA. A number of experiments qualify as *in situ* sampling devices. These include three instruments which individually collect dust grains in the coma for various types of analyses. The CIDEX instrument is a combination gas chromatograph (two pyrolysis ovens and four GC columns, each using metastable helium ionization detectors) and x-ray fluorescence spectrometer (x-ray tube and ^{244}Cm excitation sources, with a cooled high-resolution Si solid state detector). The CoMA instrument, supplied by German investigators, is a secondary ion mass spectrometer (SIMS) instrument, using a liquid metal ion source and a folded path TOFMS (Zscheeg *et al.*, 1992). The SEMPA is a miniaturized electron microscope for imaging individual microscopic dust particles, with secondary electron detector and HgI_2 x-ray fluorescence detector (Conley *et al.*, 1983). In addition, the CODEM instrument can monitor the flux, particle size distribution, electrostatic charge and velocity vector of coma dust. A neutral gas and ion mass spectrometer (NGIMS) is based upon quadrupole MS designs used in Earth-orbiting spacecraft.

A Penetrator device to have been rocketed into the nucleus from the CRAF spacecraft bus is designed to contain a gamma-ray spectrometer and a thermal/compositional analyzer for ices and low-temperature materials via differential scanning calorimetry (DSC) and evolved gas analysis (Gooding, 1989) using GC.

Titan

The Cassini mission (q.v.) to Saturn will include the Huygens probe (q.v.), which will descend through the atmosphere of Titan. Although the primary objective of the mission is to obtain atmospheric data, the probe may survive landing (or splashdown) and be able to transmit data for several minutes. Onboard is a Surface Science Package designed by British scientists (Zarnecki *et al.*, 1992). It includes an accelerometer, inclinometer, thermal and acoustic properties devices, a flotation level device, permittivity measurement device and refractometer. Through these measurements it will be possible to infer the characteristics and possibly the composition of an ocean. Originally part of this package was an x-ray fluorescence analyzer using Si(Li) and ^{55}Fe and ^{109}Cd isotope sources. Although selected on the basis of scientific merit, this portion of the experiment was beyond US budget constraints and is not being implemented.

Opportunities and options

Future *in situ* planetary experiments can include a great diversity of instruments. Based upon previous developments it is expected that x-ray, alpha, gamma ray, neutron, and mass spectrometers will be strong candidates for most future missions. Gas chromatographs and ion mass spectrometers are under advanced development, and GCMS combinations cannot be ruled out in spite of complexity. Exciting new developments in thermal analyzers, including differential scanning calorimeters and evolved gas analyzer systems, are under way for space application. Aqueous chemistry measurements capitalize on developments in solid state microchemical sensor technology. Mössbauer spectroscopy has been shown to have excellent potential for *in situ* mineralogical analyses on both the moon and Mars (Agresti *et al.*, 1992).

Because of the apparent geological diversity of Venus, a number of locations are candidates for future lander missions to determine the chemical composition of major geological units. These missions are technically very difficult because of unusually harsh environmental conditions and the nominally short lifetimes of landers.

X-ray and gamma-ray instruments are high priority for future missions where they are applicable, particularly polar orbiters. Both can also be operated on the ground, but then the x-ray would of course take advantage of artificial stimulation sources to increase sensitivity. Likewise, artificial neutron activation for gamma spectroscopy has been advocated and studied.

Advantages of sample return

For many scientific objectives, only returning samples to Earth will do, as noted above. This leads to more costly and extended missions, because of the multiplicity of events and usually the need for two separate spacecraft (outbound and return). Nonetheless, both the Soviet Union and United States have accomplished sample return from the Moon.

The array of complex, sophisticated measurements feasible only in laboratories on Earth certainly include isotopic ratio measurements and ultratrace element analyses (parts per billion or per trillion); transmission electron microscopy and atomic force imaging; Auger spectroscopy and two-step laser ion mass spectrometry; magnetic susceptibility and remnant magnetization; radiogenic nuclides assay and cosmic ray track etchings. These are, of course, only a few examples. As new techniques are developed, the value of pristine samples in reserve increases enormously. For example, the Apollo returned samples are only approximately 10% analyzed, yet still provide valuable research material for scientists and scientists in training all over the world and have been subjected to many analytical techniques that were not even available in the 1960s and 1970s when the samples were acquired.

However, the value of returned samples is much more than just the ability to accomplish intricate procedures using advanced, often finicky equipment. The quantity of data that can be generated and the number of scientists that can be involved in highly productive laboratory work can be increased by factors of tens to hundreds over that from spaceborne instruments, for the same science expenditures. In addition, new discoveries can be quickly verified by independent investigators, the foundation of the scientific method. Collaborative research combines a number of laboratories with their specialized techniques in studying the same or similar samples to magnify synergistically the understanding of the origin and history of the materials. Such collaborations have been responsible for innumerable recent scientific advances.

It must be remembered, of course, that there are many types of measurements that must be made *in situ*, even given the ability to return samples. Examples of this would be the detection and characterization of fragile components (e.g. highly reactive oxidants in Martian soil and atmosphere), samples too large to return (e.g. bedrock or sediment beds) and species that are transient (photochemical species) and would react with natural materials during the return trip. Also, samples will be subjected to a variety of unnatural (for them) environments during the rigors of the return flight, including higher temperatures, mechanical shocks, vibration and exposure to deep space radiation. In addition, the quantity of sample that can be practically returned from deep space on unmanned missions is typically of the order of 11 kg or less. The variety that can be achieved within this is significant if adequate sampling tools are included, such as chipping devices or coring drills. It is also strongly advisable to include compositional analysis instrumentation to screen samples in order to (1) determine if the samples chosen for return include a good representation of the major components and (2) assure the return of unusual materials. Sample return missions are intrinsically challenging; they are also the ultimate reward for planetary sampling science.

Benton C. Clark

Bibliography

Adler, I. (1986) *The Analysis of Extraterrestrial Materials*. New York: John Wiley and Sons.

Agresti, D.G., Morris, R.V., Wills, E.L. *et al.* (1992) Extraterrestrial Moessbauer spectrometry. *Hyperfine Int.*, **72**, 285–96.

Biemann, K., Oro, J., Toulmin, P. *et al.* (1977) The search for organic substances and inorganic volatile compounds in the surface of Mars. *J. Geophys. Res.*, **82**, 4641–58.

Clark, B.C., Baird, A.K., Rose, H.J. *et al.* (1977) The Viking x-ray fluorescence experiment: analytical methods and early results. *J. Geophys. Res.*, **82**, 4577–94.

Clark, B.C., Baird, A.K., Weldon, R.J., *et al.* (1982) Chemical composition of Martian fines. *J. Geophys. Res.*, **87**, 10059–67.
Conley, J.M., Bradley, J.G., Giffin, C.E. *et al.* (1983) Development of a miniature scanning electron microscope for in-flight analysis of comet dust, in *Microbeam Analysis – 1983* (ed. R. Gooley). pp. 177–81. San Francisco Press.
Gooding, J.L. 1989. Differential scanning calorimetry (DSC) and evolved-gas analysis (EGA) applied to planetary surface exploration, in *Proc. 18th North American Thermal Analysis Soc. Conf.* Vol. 1, (ed. I.R. Harrison) pp. 222–8.
Hoffman, J.H., Oyama, V.I. and von Zahn, L.L. (1980) Measurements of the Venus lower atmospheric composition. *J. Geophys. Res.*, **85**, 7871–81.
Horowitz, N.H. (1977) The search for life on Mars. *Sci. Am.* **237**, 52–61.
Kissel, J. Krenger, F., Clark, B.C. *et al.*, (1986) Composition of comet Halley dust particles from Giotto observations. *Nature*, **321**, 336–337.
Klein, H.P. (1979) The Viking mission and the search for life on Mars. *Rev. Geophys. Space Phys.*, **17**, 1655–62.
Kocharov, G.E., Victorov, S.V., Kovalev, V.P. *et al.* (1975) *Space Research XV*, Berlin: Akademie-Verlag.
Nature (1986) Encounters with comet Halley – the first results. **321**, No. 6067.
Nyquist, L.E., Lugmair, G. Signer, P. *et al.* (1980) Mass spectrometry–isotope dilution (MSID) of cometary solids. NASA/Johnson Space Center.
Owen, T., Biemann, K. Rushneck, D. *et al.* (1977) The composition of the atmosphere at the surface of Mars. *J. Geophys. Res.*, **82**, 4635–40.
Oyama, V.I., Carle, G.C. and Berdahl, B.J. (1977) The Viking GEX results from Chryse and Utopia surface samples. *J. Geophys. Res.*, **82**, 4669–76.
Reinhard, R. and Battrick B. (1986) The Giotto mission – Its scientific investigations. ESA SP-1077.
Surkhov, Y.A., Schcheglov, O. Moskalyeva, L. *et al.* (1982) X-ray fluorescence spectrometry on the surface of Venus. *Anal. Chem.*, **54**, 957A–966A.
Turkevich, A.L. Patterson, J.H. and Franzgrote E.J. (1967) Chemical analysis of the Moon at the Surveyor V landing site. *Science*, **158**, 635–7.
Zarnecki, J.C. McDonnell, J.A.M., Hanner, M.F. *et al.* (1992) A surface science package for the Huygens Titan probe, in *Proc. Symp. Titan*, European Space Agency SP-338, pp. 407–9.
Zscheeg, H., Kissel, J. Natour, G.H. and Vollmer, E. (1992) CoMA – an advanced space experiment for *in situ* analysis of cometary matter. *Astrophys. Space Sci.*, **195**, 447–61.

Cross references

Apollo missions
Cassini mission
Giotto mission
Huygens mission
Luna missions
Phobos mission
SNC meteorites
Surveyor missions
Titan
Vega mission
Venera missions
Viking mission

PLANETARY TORUS

Since the first observation of neutral sodium around the Jovian satellite Io (Brown, 1974), the subsequent identification of a neutral cloud extending along the orbit of Io, which followed it in its rotation around Jupiter (Matson *et al.* 1978), and the discovery of ionized sulfur and oxygen tori surrounding Io's orbit (Kupo, Meckler and Eviatar, 1976; Pilcher and Morgan, 1979), a significant number of planetary tori have been discovered in the vicinity of the satellites of the giant planets Jupiter, Saturn and Neptune. These tori may consist of either neutral or ionized species. They may completely surround the planet or may only consist of partial arcs; they may follow the satellite's orbit or lie in a different plane. However, planetary tori are found only around magnetized planets, with satellites embedded in the magnetosphere. This indicates that, despite this wide variety of morphological and physical differences, the planetary tori are a single class of planetary objects. Reviewing the various tori observed so far, we will show that their differences are related to the compositional characteristics of the satellite, the dynamical characteristics of the planetary magnetosphere and the geometry of the satellite–magnetic field system.

Origin of planetary tori

The interaction between a satellite, its neutral environment, its plasma torus and the magnetosphere is based on feedback loops which insure the stability of the system. Suppose a satellite exists in a magnetosphere without an initial plasma population (this simplified scenario is in fact not realistic, since some plasma from the solar wind and from the planetary ionosphere is always present in a magnetosphere). Molecules and grains can be sputtered out from the surface of the satellite or from an atmosphere by micrometeroid impact, by collisions with high-energy particles from the magnetosphere, by photosputtering, and by thermal escape of gas from an atmosphere. This type of source provides neutral gas in the vicinity of the satellite, roughly corotating with it. The fastest molecules can escape the satellite's gravitational field and flow into a toroidal volume around its orbit under the planet's gravity, forming a neutral torus (or a neutral torus segment depending on their lifetime). This neutral gas begins to be ionized, essentially by photoionization and interaction with the particles of the radiation belts. Although produced at a slow rate, these freshly created ions behave as a plasma 'frozen' into the planetary magnetic field and are dragged by the field lines into rotation. This is commonly called the 'pick-up' phenomenon. The magnetic field lines rotate roughly at the planet's velocity ('corotation'), i.e. significantly faster than the satellite on its Keplerian orbit, so that the newly picked up ions acquire an energy close to the corotation energy (in the range of several tens to a few hundred eV, depending essentially on the mass of the ion and the radial distance of the pick-up). Under the combined effect of the gravitational and centrifugal forces, the ions remain confined close to the centrifugal equatorial plane between the rotational and the magnetic equatorial planes (Richardson, Eviatar and Siscoe, 1986, and references therein). A fraction of these corotating ions impact their source satellite or its atmosphere and increase the population of neutrals in the corona and in the neutral cloud. Another fraction collide with electrons and energize them such that they become a new significant source of ionization of the neutrals, in addition to the initial photoionization. If this feedback loop (illustrated in Figure P16 for the case of Io) is efficient enough, the neutral cloud and the plasma can theoretically become self-supporting (Eviatar, Kennel and Neugebauer, 1978; Huang and Siscoe, 1987).

This oversimplified scenario does not take into account the necessary balance between plasma torus sources and losses required to attain a steady state equilibrium, nor the interactions of the tori with the surrounding magnetosphere (Figure P17). The hot ions can be lost to the torus by charge exchange with thermal neutrals, mainly from the neutral clouds. This results in the production of a thermal ion, immediately picked up by the magnetic field, and of a fast neutral which leaves the system at the corotation velocity. These neutrals are a significant source of plasma for the distant magnetosphere, where a fraction can be ionized again (Barbosa and Eviatar, 1986), and even for the interplanetary medium: a sodium nebula has recently been discovered around Jupiter extending beyond 400 R_J (Flynn, Mendillo and Baumgardner, 1992). The density of the torus is not affected, and the net effect concerns mainly the composition (the new ion can be different from the initial one) and the energy budget. Plasma can also be lost by recombination and radial transport into the magnetosphere. Centrifugally driven transport of heavy ion plasma controls the steady state Io plasma torus and is a major source of plasma in the magnetosphere of Jupiter (Siscoe and Summers, 1981). Radial transport also seems to play a major role in the control of the Triton torus–Neptune magnetosphere system (Richardson *et al.*, 1991). At Uranus convective transport, externally driven by the solar wind, removes any plasma from the satellites, and prevents the formation of a plasma torus (Vasyliunas, 1986). By contrast, the density of the 'water group' plasma torus surrounding Dione and

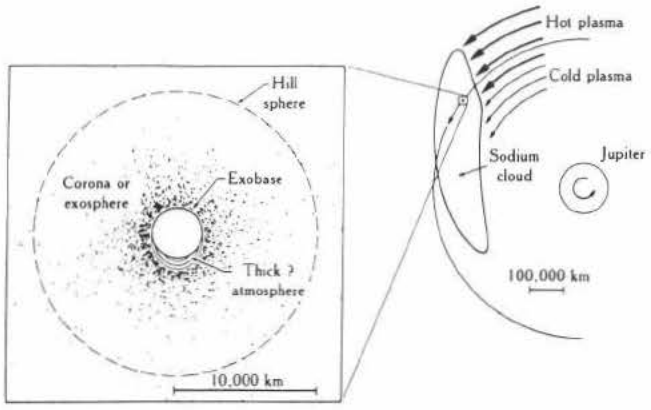

Figure P16 Schematic view of the atmosphere and sodium cloud of Io. To the left: Io's vicinity (the Hill sphere is the effective limit of Io's gravity). To the right, the neutral sodium cloud contour. The arrows represent the corotating plasma, traveling at 75 km s^{-1} past the neutrals that orbit Jupiter at 17 km s^{-1}. The cloud lies preferentially inside Io's orbit because the plasma is cooler there and less able to ionize the sodium atoms. Inside Io's orbit the cloud extends forward only, because atoms closer to Jupiter travel faster than Io. (From Schneider, Smyth and McGrath, 1989.)

Tethys is controlled by recombination (Richardson, Eviatar and Siscoe, 1986).

Finally, a plasma torus can also act as a sink for high-energy magnetospheric particles (among which some originally came from the torus plasma itself). The dense cold plasma of the torus favors resonant interaction of the particles with electromagnetic waves, resulting in pitch-angle diffusion, precipitation along field lines into the planetary high-latitude atmosphere and, ultimately, excitation of auroral emissions (Goertz, 1980; Thorne, 1983; Prangé, 1991; and references therein).

Observational techniques

Remote sensing by optical emissions

Although so far only applicable to the study of the Io torus (because of insufficient brightness of the other tori), remote sensing from ground-based telescopes is the most widely used tool for the study of planetary tori. It is through the detection of the D resonance doublet of sodium in the spectrum of Io that the Io sodium cloud was discovered in 1972 (Brown, 1974); all the information on the neutral and ionized Io tori was derived from observation of their optical emissions until the Voyager encounters in 1979. Remote sensing from space has also been widely used from 1979 on, with the observations of the Ultraviolet Spectrometer (UVS) during the Voyager 1 and 2 encounters with the Jupiter and Saturn systems, and of the Earth orbiting International Ultraviolet Explorer (IUE), still in operation, and since 1992, of the Hubble Space Telescope (HST) and of the Extreme Ultraviolet Explorer (EUVE). The neutral emission lines are due to resonance scattering of allowed transitions from the solar lines, whereas the emissions from the ionized species are excited by collisions with electrons. Remote imaging of the tori emission gives access to the morphology of the tori (the interpretation of the many 'asymmetries' of the Io tori and of their temporal variation has been fundamental in the understanding of the system). High-resolution spectroscopy provides information on the composition, density, temperature and thermodynamical equilibrium (by the study of the line intensity ratios), and on the velocity fields by the observation of Doppler shifts.

In addition, information on the integrated electron density in the Io torus has also been obtained by radio occultation techniques on the Voyager and Ulysses missions.

In situ measurements of plasma parameters

The deep space missions to the giant planets included instrumentation dedicated to the measurement of the charged particle distribution functions (density, composition, energy, flow direction, temperature) in various energy ranges, and in particular below a few keV. The *in situ* determination of the plasma frequency by the electromagnetic wave analyzers also provided the total plasma density. This has been the only means of identification and characterization of the distant or tenuous tori, whose emissions are too faint to be observed, such as the inner plasma torus in the magnetosphere of Saturn or the suspected Europa torus at Jupiter. Although not directly detected by the Voyager spacecraft, the Triton partial torus has been recognized by the analysis of the ions it has released in the 'nearby' magnetosphere.

A large body of information has been obtained on the Io plasma tori by comparing the *in situ* measurements of the Voyagers with the optical data. Similarly, the recent crossing of the torus by Ulysses has already begun to provide new and valuable data, in particular far from the equatorial plane, which can be correlated to remote observations (see Ulysses mission).

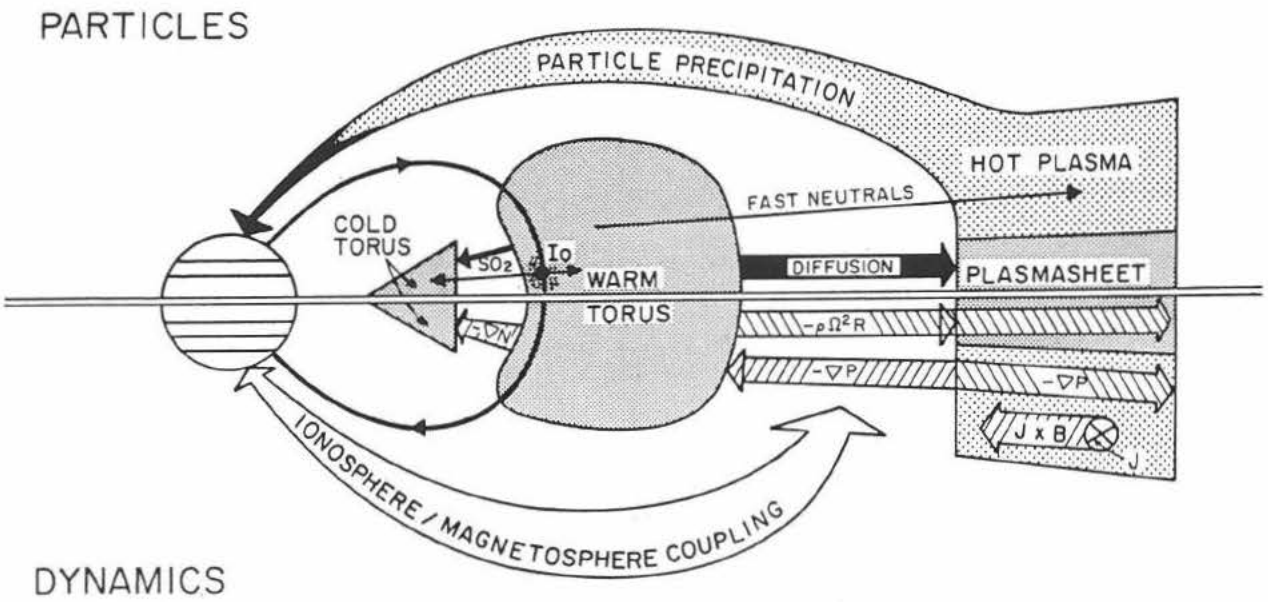

Figure P17 Coupling between the Io tori, the atmosphere and the magnetosphere of Jupiter. (From Bagenal 1989.)

Io tori: a model study of satellite–magnetosphere interactions

Io (q.v.), the innermost Galilean satellite of Jupiter, experiences strong time variable gravitational effects from Jupiter and Ganymede, resulting in tidal heating and volcanism. The volcanic activity was first discovered by imaging with Voyager in 1979, and provides to the tori mainly sulfur and oxygen, at a total rate of around 10^3 kg s^{-1} (a few 10^{28} atoms s^{-1}), with traces of sodium and potassium. This gives Io a well-developed atmosphere and ionosphere. The resulting tori are the densest and the brightest in the solar system. They are easily observable from Earth and they have been visited three times by deep space missions. Consequently a large body of data has been gathered on the Io tori, and an intense theoretical effort of modeling is taking place, making the Io tori a reference model for planetary tori.

Neutral clouds and tori

The observations and the physics of the neutral Io clouds have produced a large body of literature, including many review papers (Schneider, Smyth and McGrath, 1989; Thomas, 1992; also McNutt, 1991).

Io has a significant atmosphere of SO_2 (with a column density of 10^{15} to 10^{17} cm^{-2}), with some neutral sulfur and oxygen ($\geq 10^{12}$ cm^{-2}). Through the mechanisms detailed above, part of these neutrals escape and give rise to a neutral cloud extending along the orbit of Io, at roughly six Jovian radii (R_J) from Jupiter. However, these neutral clouds are extremely tenuous and their resonance lines very faint (a few rayleighs or less). Although sodium is a very minor constituent in the atmosphere of Io (10^{12} cm^{-2}), its resonance D lines at $\approx$ 5890–5896 Å are extremely bright (thousands of rayleighs in the vicinity of Io). The sodium cloud has been used as a model to study the neutral tori.

The 'banana-shaped' sodium cloud extends over several tens of degrees along Io's orbit in the rotational equatorial plane (Figure P15). Its size is limited by the lifetime of sodium atoms against ionization (a few hours in the equatorial plane). Models of its exact shape depend in particular on the distribution of the velocity of the escaping atoms and of the ionizing electrons (Smyth and Combi, 1988). By contrast, the lifetime of neutral oxygen and sulfur is much longer (tens of hours), giving rise to complete neutral tori.

An east–west asymmetry is present in the emission strength measured near Io, with an excess of $\approx$ 20% at western elongation. This has been attributed to solar radiation pressure effects, or to an asymmetric atmospheric shielding of the surface of Io to particle impact. It was also observed that the emission is strongest on the side of Io opposite to the Jovian magnetic equator (a north–south asymmetry modulated with a 13-h period). This has been explained by an increased ionization of the neutrals by the plasma torus particles which lie in the centrifugal equatorial plane, about 5° from the orbital plane of Io in the direction of the magnetic equator. Finally, the intensity varies also as a function of heliocentric orbital longitude, due to the variation of the solar flux when the resonance line is shifted along the gradient of the large solar Fraunhofer line, an effect not related to the physics of the system itself. Characteristic fast jets of neutral sodium (10 to 100 km s^{-1}) are regularly observed escaping from the cloud of slow sodium (Figure P18). They are now

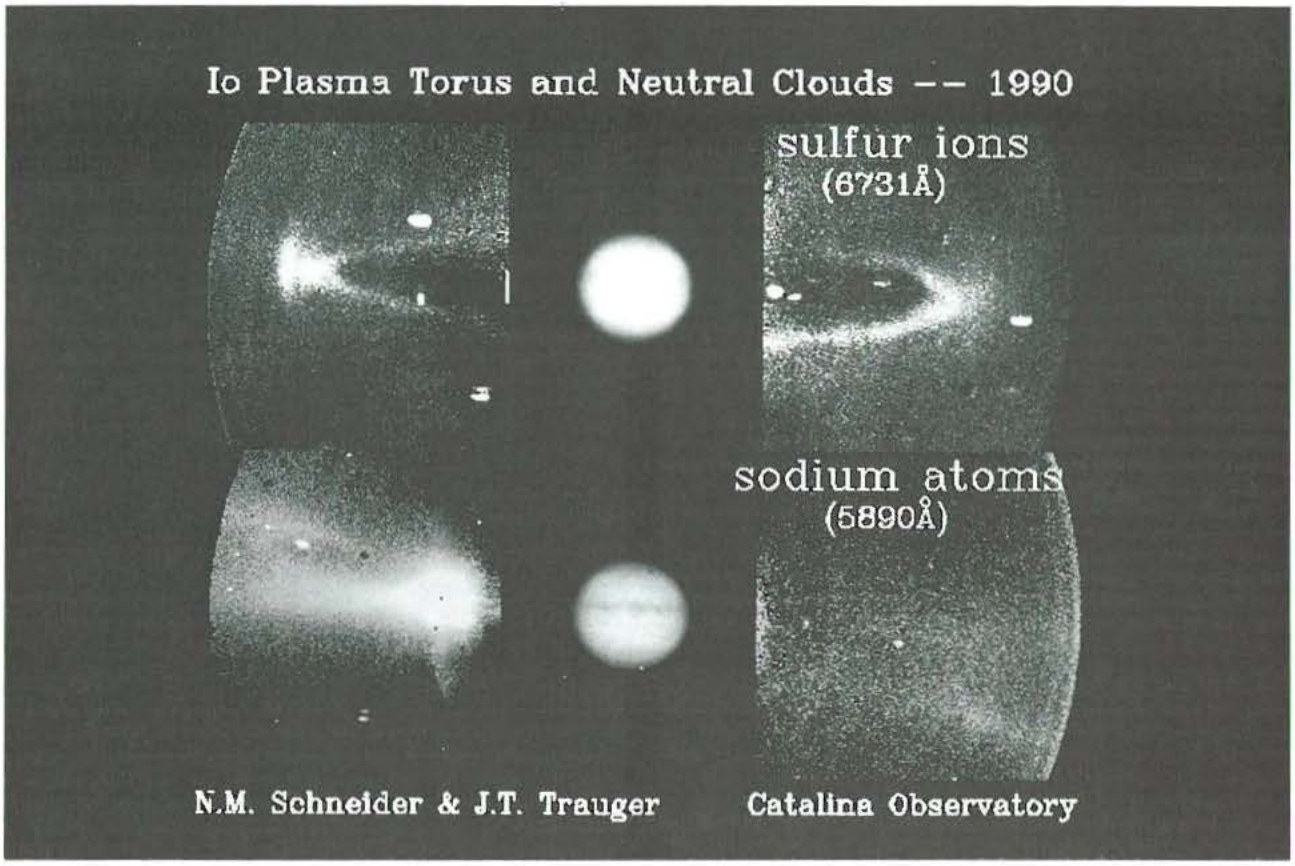

Figure P18 Ground-based observations of the Io tori. Top: the S^+ (sulfur) plasma torus. The bright narrow feature extending on both sides of the equatorial plane is the 'ribbon' (inner edge of the warm torus). The cold torus, extending planetwards, is separated from the ribbon by an emission gap. Bottom: the Na cloud of slow sodium (elongated spot ahead of Io) and a torus of fresh Na atoms just charge exchanged from picked-up ions (faint bent trace). The bright spot in the left panel, connected to the sodium cloud, is the solar flux scattered by Io. Jupiter's light (center panel) has been attenuated by an absorbing film in both pictures. (N.M. Schneider, personal communication.)

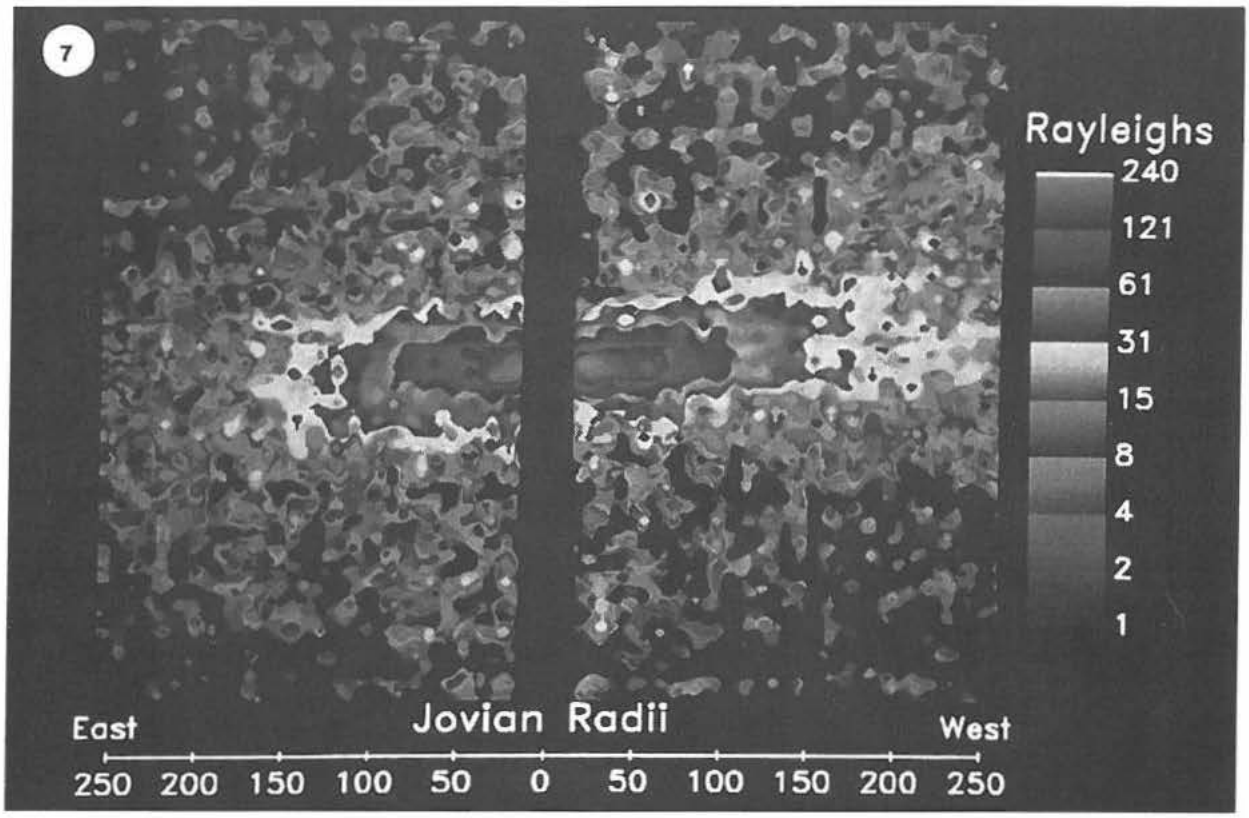

Figure P19 A ground-based composite image of the Jovian environment in the D1–D2 lines of neutral sodium from a series of drift scan spectra. The sodium nebula is evident in Jupiter's equatorial plane (tilted by 5° at the time of the observations), extending to several hundred Jovian radii in the interplanetary space. As in the case of the tori, an east–west asymmetry is visible. The dark region centered on Jupiter comes from the intensifier being turned off, to avoid damage due to light from Jupiter's bright disk. (From Flynn, Mendillo and Baumgardner, 1992.)

attributed to dissociative recombination of fresh sodium-bearing ions in the plasma torus, and are a source of Iogenic neutrals in the Jovian magnetosphere and the interplanetary medium (Barbosa and Eviatar 1986; Flynn, Mendillo and Baumgardner 1992), as shown on Figure P19.

Plasma tori

The remote optical observations and *in situ* plasma measurements have both given evidence of high plasma density in a toroidal region between 5 and 7.5–8 R_J from Jupiter, centered on the centrifugal equator, with a thickness scale height of $\approx 1\ R_J$. Both techniques have identified two main regions (Figures P17 and P20). The inner or 'cold' torus is dominated by singly ionized species (O^+, S^+), and the corresponding electron temperature is of the order of 10^4 K. It is located inside Io's orbit with a peak density of about 1000 cm^{-3} at the distance of $\approx 5.3\ R_J$, and is closely confined to the equatorial plane. In the outer or 'warm' torus multiple ionization dominates (S^{++},O^{++},S^{3+}), and the electron temperature is $\approx 6 \times 10^5$ K. The warm torus in fact extends inwards beyond Io's orbit, and one can define a third region, the 'warm inner torus' confined between 5.7 and 5.9 R_J, where the peak density, $\approx 3 \times 10^3\ cm^{-3}$, exceeds by a factor of three the peak density in the outer torus (at 6 R_J). This narrow region had been independently observed as a very bright feature in the ground-based images and called the 'ribbon'. Efforts have been concentrated in the past decade on modeling of the Voyager data (Bagenal and Sullivan, 1981), of the optical images (e.g. Morgan, 1985) and of the thermodynamical equilibrium of the species (e.g. Smith and Strobel, 1985), in order to ascertain the characteristics of the Io tori from the observations. Recent reviews of such studies can be found in Strobel (1989), Bagenal (1989), Thomas (1992) and Spencer and Schneider (1996).

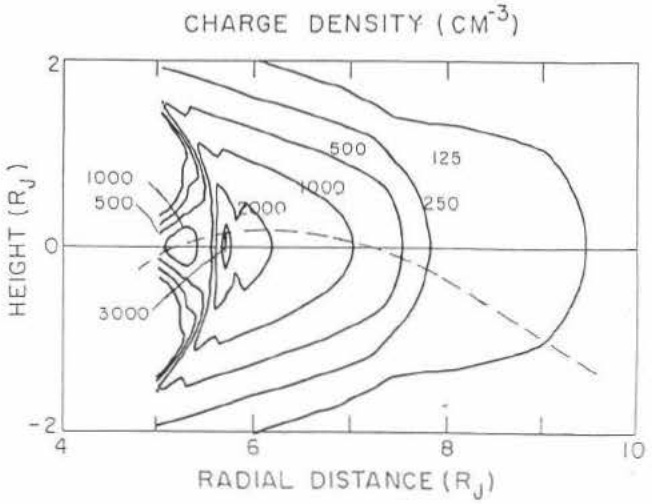

Figure P20 Isocontours of the ion density in the Io tori in a meridional plane derived from the plasma probe and UV spectrometer on Voyager. The large area on the right is the warm outer torus. The small secondary maximum on the left is the cold torus. The warm inner torus, or 'ribbon', observable from ground-based telescopes, is the region of sharp density gradients in between. The dashed line represents Voyager trajectory through the torus. (F. Bagenal, personal communication.)

The Io plasma torus radiates copious amounts of energy in the EUV, UV and visible lines through electron impact. At the epoch of the Voyager encounters, the total radiated power was of the order of $3–6 \times 10^{12}$ W. The traditional energy source (pick-up of fresh ions) is insufficient to fuel this power loss. To solve this 'energy crisis', it has been proposed that part of the high-energy magnetospheric ions diffuse inward into the hot torus and transfer their energy to electrons by collision (Smith *et al.*, 1988). An alternative (or complementary) magnetospheric source of energy to the warm torus has been proposed in the form of a flow of hot ionospheric electrons secondary to the precipitation of magnetospheric particles in the outer torus (e.g. Thorne, 1983). These theories partly conflict with the early theories of a self-sustaining torus. Finally, the outer torus seems to be a sink for high-energy magnetospheric particles (Gehrels and Stone, 1983; Prangé, 1991), presumably through pitch-angle diffusion. Reviews of the complex coupling of the outer Io torus with the Jovian magnetosphere can be found in Thorne (1983) and Bagenal (1989).

Torus properties vary with longitude, latitude and local time. These variations, mostly poorly understood so far, stimulate theoretical studies on the interaction of the torus with the magnetosphere. A local time asymmetry in the EUV brightness of the torus, with maximum intensity at western elongation, has been attributed to a variation in electron temperature. The existence of a dawn-to-dusk electric field across the magnetosphere has been proposed to account for this increased electron temperature (Barbosa and Kivelson, 1983; Goertz and Ip, 1984).

Periodic longitudinal variations in the brightness of the short-lived species (such as S^{+1}) have been reported with maxima near 180–250°, not supported by the *in situ* Voyager measurements of total plasma density. These variations seemed to be better organized in a coordinate system rotating 3% slower than 'system III' (corotating with the magnetic field), giving rise to controversial interpretations. The very recent identification of denser plasma bubbles rotating in the inner and outer plasma tori by the radio experiment onboard the Ulysses spacecraft (Reiner *et al.*, 1993) might provide an explanation of this phenomenon. Recently the radial distance of the torus from Jupiter has also been found to vary with longitude, roughly in phase with the variation of the surface magnetic field. A dawn-to-dusk asymmetry of this effect is also observed.

Finally, it is worth noting that the Io plasma tori were optically very faint at the epoch of the Pioneer encounters (1973–74). This considerable long-term variation of torus activity may be related to a similar variation of the Jovian UV auroral activity, which was hardly detectable by the Pioneer spectrometers, and reached tens to hundreds of kilorayleighs since the beginning of the 1980s.

Other planetary tori

Among the magnetized planets of the solar system, only Jupiter, Saturn and Neptune possess planetary tori. Mercury does not have a satellite. The Earth's Moon, in addition to releasing little matter through surface sputtering, orbits at a distance of 60 R_E from Earth, and spends less than 10% of its orbital period in the planet's magnetotail. By contrast, Uranus has five large satellites embedded in the magnetosphere, between 5 and 23 R_U. Ices seem to be present on all of them, and they must be sources of water and other volatiles. However, the motion of the plasma in the Uranian magnetosphere is controlled by solar wind-driven convection, rather than by corotation as in the case of Jupiter, and the odd geometry of the system (the axis of rotation is close to the ecliptic plane and, at the time of the Voyager flyby in 1986, sunward directed; the magnetic axis is tilted by $\approx 57°$ from the rotation axis, and rotating in ≈ 17 h) results in an efficient sweeping out of the satellite plasma within a few hours, preventing the formation of any plasma torus (Vasyliunas, 1986; Richardson *et al.*, 1991), and hence of any self-sustaining neutral torus.

Jupiter

The existence of a plasma torus generated by the icy satellite Europa has long been suspected, but until recently there was no conclusive evidence of its existence. Very recent reanalysis of Voyager data now indicate the presence of hot, freshly picked-up ions in the vicinity of the orbit of Europa ($\approx 9.5\ R_J$), an excess of O^{++} with respect to sulfur and the presence of H_3O^+, confirming the inference of a torus of 'water group' ions (Bagenal *et al.*, 1992). This species can be expected from sputtering of the surface, but alternatively might confirm the role of tidal heating in exciting 'geyser-like' activity as suggested in Howell and Sinton (1989).

Saturn

One of the major differences between the magnetospheres of Jupiter and Saturn is the absence at Saturn of an Io-like satellite able to outgas large amounts of volatiles in the dense inner magnetosphere. By contrast, small icy satellites and rings can release smaller amounts of 'water-group' molecules in the inner magnetosphere (by sputtering and micrometeorid impact). The one satellite with an atmosphere and a significant gas output is Titan, which orbits at 20 R_s, well outside the main plasma bodies of the magnetosphere.

Essentially all observational information on the magnetosphere of Saturn comes from the Pioneer and Voyager encounters. This explains why, despite a large amount of data analysis and theoretical work, many unsolved questions remain still. The information comes from the *in situ* particle and wave data and, for the neutral Titan torus only, from remote sensing with the Voyager 1 and 2 UVS instrument. Figure P21 indicates schematically the location of the main neutral and plasma tori in the magnetosphere of Saturn. Recent work and reviews on the state of the art can be found in Richardson and Eviatar (1988), Eviatar, Podolak and Richardson (1990), McNutt (1991), Ip (1992) and Gombosi (1992).

Titan torus

As early as 1973 McDonough and Brice predicted the existence of a measurable neutral hydrogen torus in the vicinity of Titan's orbit. Although this was based on an erroneous composition of Titan's atmosphere, the Voyager 1 UVS instrument detected a 100 raleigh Lyman α emission from an extended region inside Titan's orbit (Broadfoot *et al.*, 1981). This was interpreted as resonance scattering of solar Lyman α by an atomic hydrogen torus, of average density 10–20 cm^{-3}, $\approx \pm 3–10\ R_s$ thick, and extending radially from 8 to 25 R_s in the equatorial plane, consistent with a Titanogenic origin. From the discovery by Voyager of a thick atmosphere, composed mainly of molecular nitrogen and methane (with surface pressure ≈ 1 bar, and column densities $> 10^{16}$ cm^{-2} near the exobase), considerable efforts focused on the modeling of such a torus. Photodissociation and electron impact dissociation of CH_4 and N_2 provide mainly hot atomic hydrogen and nitrogen (H and N). A large fraction can escape Titan's gravity. Model estimates of the escape rates for each species have been derived in the range 2×10^{26} to 3×10^{27} atoms s^{-1} with escape velocities of a few kilometers per second (Strobel and Shemansky, 1981; Barbosa, 1987; Ip, 1992, and references therein). A colocated H_2 torus (undetectable so far) of similar density (a few tens per cubic centimeter) and a N torus, about five times fainter, are also predicted. The existence of local time asymmetries due to solar pressure effects are also discussed.

Ionization of the neutrals in these tori must provide keV picked up H^+ and N^+ ions (Eviatar, Podolak and Richardson, 1990; Barbosa, 1987; Gombosi, 1992). Warm, keV 'light' and 'heavy' ions in partial corotation, presumably H^+ and N^+, have been observed by the plasma probes on Pioneer 11, and Voyager 1 and 2, with low densities ≈ 0.1 to 1 cm^{-3} outward of 8 R_s (Lazarus and McNutt, 1983). Barbosa (1987) argues that this faint N^+ Titan torus, like the Io plasma torus at Jupiter, is a major plasma source for the magnetosphere, supplying energy for the observed auroral precipitation.

This 10 year old, well-documented picture of the Titan hydrogen torus (and other associated tori) might suffer major changes in the near future: Shemansky and Hall (1992) have reanalysed Voyager 1 and 2 UVS data. They state that Lyman α emission is distributed throughout the whole magnetosphere of Saturn inside the orbit of Titan; that the hydrogen atoms originate from Saturn's exosphere; and that any Titanogenic H torus would contribute at most 30 rayleighs of Lyman α, and fill the 18.5–20.5 R_s region only.

Inner plasma tori

In the inner magnetosophere the moons Enceladus (4 R_s), Tethys (4.9 R_s), Dione (6.2 R_s) and Rhea (8.7 R_s) have icy surfaces from which neutrals can be sputtered out. These neutrals can be dissociated or ionized. Removal of these ions from the tori as fast neutrals can occur from charge exchange or recombination at Tethys and Dione, or by transport processes at Rhea. The net result is the formation of tori containing H, H_2, O, OH, H_2O and O_2, and their ions. The Pioneer and Voyager plasma probes indeed measured a mixed proton and water-group ion plasma (O^+, OH^+ and H_2O^+)

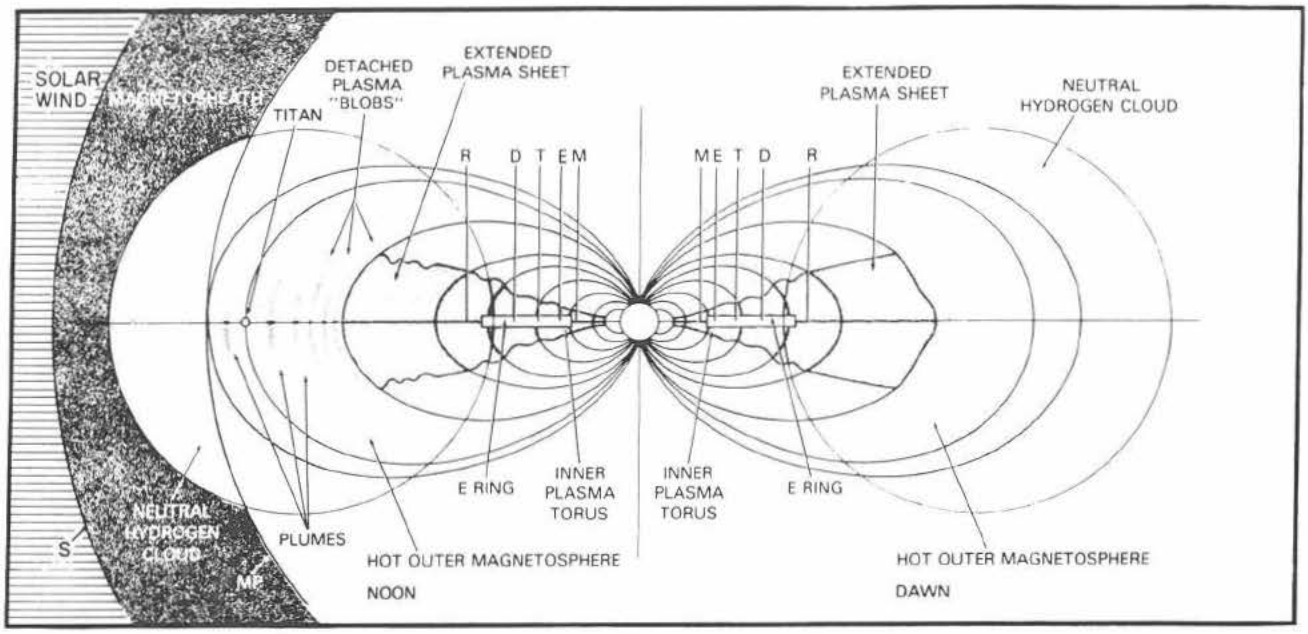

Figure P21 Schematic representation of the magnetosphere of Saturn with the location of the main neutral and plasma tori. The icy satellites are identified by their initial: Mimas (M), Enceladus (E), Tethys (T), Dione (D) and Rhea (R). (From Sittler, Ogilvie and Scudder, 1983.)

between 2.7 R_s (closest approach) and ≈ 7 R_s. The plasma is roughly corotating with the magnetic field (energies ≈ 100 eV), and is strongly confined to the equatorial plane with a half-width of the heavy ion tori ≤ 1 R_s (with a somewhat larger thickness for the protons). Heavy ions densities of $\approx$ 20–40 cm^{-3} were observed near the equatorial plane at the orbits of Tethys and Dione, increasing to $\approx$ 150–200 cm^{-3} near the rings at 2.8 R_s (Lazarus and McNutt, 1983). The average heavy ion and proton density is roughly 12 and 2 cm^{-3}, respectively in the Tethys and Dione torus, and ≈ 2 cm^{-3} for both in the Rhea torus (Richardson, Eviatar and Siscoe, 1986). The presence of tenuous neutral tori of densities $\approx$ 2–8 cm^{-3} was theoretically predicted from these observations. As in the case of the Titan torus, part of this picture, and of the corresponding models, may be overthrown by the recent remote detection (with HST) of neutral OH in the vicinity of the orbit of Thetys with a density of 160 cm^{-3}, more than 20 times the previous estimates (Shemansky *et al.*, 1993).

Ring hydrogen torus

An early indication of the presence of an atomic hydrogen torus surrounding the rings of Saturn has been obtained via the detection of Lyman α emission with a rocket flight and with Copernicus (Weiser, Vitz and Moos, 1977; Barker *et al.*, 1980). The observation of 360 R of Lyman α by UVS during the Voyager 1 fly by confirmed the existence of a neutral hydrogen ring torus. The H average density should be 600 cm^{-3} if distributed in a torus of circular cross section of radius 1 R_s. This hydrogen was supposed to originate from sputtering of the ices in the ring material. However, the recent suggestion of a large exospheric source of atomic hydrogen filling the whole magnetosphere (see above), if confirmed, could probably also account for these observations without the need of an extra ring torus.

Neptune

Triton torus

The presence of nitrogen and methane frosts on Triton (at 14 R_N from Neptune), and the indication of a sizable magnetosphere, was inferred from IR spectroscopy and microwave observations a few years before the Voyager 2 encounter with Neptune. This analogy with Titan led Delitsky, Eviatar and Richardson (1989) to predict the existence of a measurable Triton plasma torus. The fly by of Neptune on 25 August 1989 found only indirect evidence of such a torus (whose density was below the detection threshold of the plasma detectors), in the form of the detection of H^+ and N^+ ions inside Triton's orbit, and of the observation of a faint, longitudinally asymmetric UV aurora. The discovery of the unexpected magnetic field geometry (dipole axis tilted by 47° from the planet's spin axis, and center offset by ≈ 0.5 R_N), combined with the inclination of the orbit of Triton by 22°, revealed a novel configuration, with Triton's orbit crossing a wide range of magnetic L shells from L = 14 in the magnetic equatorial plane, to more than 100 at high latitude (the McIlwain parameter L of a magnetic field line is the equatorial distance of the equivalent dipole field line, expressed in planetary radii; a magnetic L shell is the locus of the field lines with the same L

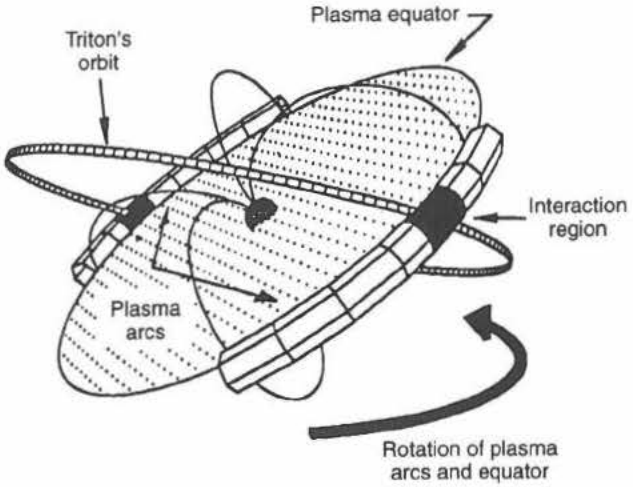

Figure P22 Formation of two torus segments (plasma arcs) in Neptune's plasma equator. Triton's orbit, tilted by $\approx$ 22° from Neptune's spin equator, intersects magnetic field lines from L $\approx$ 14 (near the plasma equator, tilted $\approx$ 40° from the spin equator) to L $\approx$ 100 (at high latitude). The subsequent ionized species are more confined and denser close to the minimum L flux tube, intersected in the longitude range 140–210° and 310–325°. (From Broadfoot *et al.* 1989, copyright 1993 by permission American Astronomical Society.)

parameter obtained by rotation around the planet). The subsequent formation of arcs of plasma in the centrifugal equator was inferred by Broadfoot *et al.* (1989). These arcs are longitudinally limited to the intersections of Triton's orbit with the minimum L shells, 14 to 15 (Figure P22), and could explain the morphology of the auroras. Voyager 2 also revealed the existence of a thick atmosphere (14 μbar at surface level), dominated by N_2, with traces of CH_4 and H_2 and of a dense ionosphere (with a peak density of $\approx 4 \times 10^4$ cm^{-3}, and composed primarily of N^+). Richardson *et al.* (1991) estimate that a neutral H cloud, similar to Titan's H torus, must form by thermal escape along Triton's orbit, extending inwards to L = 8, with average density of ≈ 500 cm^{-3} (other estimates range from 30 to 1000 cm^{-3}). The ionization of this torus could provide the source of the H^+ 'light ions' observed beyond L = 8, whereas the 'heavy' N^+ ions observed would be directly injected from the ionosphere at Triton. These estimates are consistent with the plasma measurements inside L = 13. By contrast, Richardson *et al.* (1991) could not find in the plasma data any confirmation of the longitudinal asymmetry of the plasma torus. However, the observations in the magnetosphere of Neptune have intrinsic limitations, and they are still very recent. Additional analysis and theoretical studies to come might change the present picture.

Renée Prangé

Bibliography

Bagenal, F. (1989) Torus–magnetosphere coupling, in *Time Variable Phenomena in the Jovian System* (eds M.J.S. Belton, R.A. West and J. Rahe) Washington: NASA SP-494, pp. 196–210.

Bagenal, F. and Sullivan J.D. (1981) Direct plasma measurements in the Io torus and inner magnetosphere of Jupiter. *J. Geophys. Res. A*, **86**, 8447–66.

Bagenal, F., Shemansky, D.E., McNutt, R.L., Jr *et al.* (1992) The abundance of O^{++} in the Jovian magnetosphere. *Geophys. Res. Lett*, **19**, 79–82.

Barbosa, D.D. (1987) Titan's atomic nitrogen torus: inferred properties and consequences for the Saturnian aurora. *Icarus*, **72**, 53–61.

Barbosa, D.D. and Eviatar, A. (1986) Planetary fast neutral emission and effects on the solar wind: a cometary exosphere analog. *Astrophys. J.*, **310**, 927–36.

Barbosa, D.D. and Kivelson, M.G. (1983) Dawn–dusk asymmetry of the Io plasma torus. *Geophys. Res. Lett.*, **10**, 210–3.

Barker, E.S., Cazes, S. Emerich, C. *et al.* (1980) Lyman alpha observations in the vicinity of Saturn with Copernicus. *Astrophys. J.*, **242**, 383–94.

Broadfoot, A.L., *et al.* (1981) Extreme ultraviolet observations from Voyager 1 encounter with Saturn. *Science*, **212**, 206–11.

Broadfoot, A.L., *et al.* (1989) Ultraviolet spectrometer observations of Neptune and Triton. *Science*, **246**, 1459–66.

Brown, R.A. (1974) Optical line emission from Io, in *Exploration of the Planetary System* (eds A. Woszczyk and C. Iwaniszewska) Boston: Reidel, pp. 527–31.

Delitsky, M.L., Eviatar, A. and Richardson J.D. (1989) A predicted Triton plasma torus in Neptune's magnetosphere. *Geophys. Res. Lett.*, **16**, 215–8.

Eviatar, A., Kennel, C.F. and Neugebauer, M. (1987) Possible origins of the variability in Jupiter's outer magnetosphere. *Geophys. Res. Lett.*, **5**, 287–9.

Eviatar, A., Podolak M. and Richardson, J.D. (1990) Atomic and molecular hydrogen from Titan in the Kronian magnetosphere. *J. Geophys. Res. A*, **95**, 21007–16.

Flynn, B., Mendillo, M. and Baumgardner, J. (1992) Observations and modeling of the Jovian remote neutral sodium. *Icarus*, **99**, 115–30.

Gehrels, N. and Stone, E.C. (1983) Energetic oxygen and sulfur ions in the Jovian magnetosphere and their contribution to the auroral excitation. *J. Geophys. Res. A*, **88**, 5537–50.

Goertz, C.K. (1980) Proton aurora on Jupiter's nightside. *Geophys. Res. Lett.*, **7**, 365–8.

Goertz, C.K. and Ip, W.H. (1984) A dawn–dusk electric field in the magnetosphere of Jupiter. *Planet Space Sci.* **32**, 179–85.

Gombosi, T.I. (1992) Mass loading at Titan and comets, in *Symposium on Titan*, (ed. B. Kaldeich) Paris: ESA SP-338, pp. 255–61.

Hill, T.W. and Dessler, A.J. (1990) Convection in Neptune's magnetosphere. *Geophys. Res. Lett.*, **17**, 1677–80.

Howell, R.R. and Sinton, W.M. (1989) Io and Europa: the observational evidence for variability, in *Time Variable Phenomena in the Jovian System* (eds M.J.S. Belton, R.A. West and J. Rahe). Washington: NASA SP-494, pp. 47–62.

Huang, T.S. and Siscoe, G.L. (1987) Types of planetary tori. *Icarus*, **70**, 366–78.

Ip, W.H. (1992) Plasma interaction of Titan with the Saturnian magnetosphere: a review of critical issues, in *Symposium on Titan* (ed. B. Kaldeich). Paris: ESA SP-338, pp. 243–53.

Kupo, I., Meckler, Y. and Eviatar, A. (1976) Detection of ionized sulfur in the Jovian magnetosphere. *Ap. J. Lett.*, **205**, L51–3.

Lazarus, A.J. and McNutt, R.L., Jr (1983) Low-energy plasma ion observation in Saturn's magnetosphere. *J. Geophys. Res. A*, **88**, 8831–46.

Matson, D.L., Goldberg, B.A., Johnson, T.V. and Carlson, R.W. (1978) Images of Io's sodium cloud. *Science*, **199**, 531–3.

McDonough, T.R. and Brice, N.M. (1973) A Saturnian gas ring and the recycling of Titan's atmosphere. *Icarus*, **20**, 136–45.

McNutt, R.L., Jr (1991) The magnetospheres of the outer planets. *Rev. Geophys. Suppl.* US National Report to IUGG, 985–97.

Morgan, J.S. (1985) Models of the Io torus. *Icarus*, **63**, 243–65.

Pilcher, C.B. and Morgan, J.S. (1979) Detection of singly ionized oxygen around Jupiter. *Science*, **205**, 297–8.

Prangé, R. (1991) Jovian UV aurorae, IR aurorae, and particle precipitation: a common origin? *Astron. Astrophys.*, **251**, L15–8.

Reiner, M.J., Fainberg, J., Stone, R.G. *et al.* (1993) Source characteristics of Jovian narrow-band kilometric radio emissions. *J. Geophys. Res. A*, **98**, 13163–76.

Richardson, J.D., and Eviatar, A. (1988) Observational and theoretical evidence for anisotropies in Saturn's magnetosphere. *J. Geophys. Res. A*, **93**, 7297–306.

Richardson, J.D., Eviatar, A. and Siscoe G.L. (1986) Satellite tori at Saturn. *J. Geophys. Res. A*, **91**, 8749–55.

Richardson, J.D., Belcher, J.W., Zhang, M. and McNutt R.L. Jr (1991) Low-energy ions near Neptune. *J. Geophys. Res. A*, **96**, 18993–9011.

Schneider, N.M., Smyth, W.H. and McGrath, M.A. (1989) Io's atmosphere and neutral clouds, in *Time Variable Phenomena in the Jovian System* (eds M.J.S. Belton, R.A. West and J. Rahe). Washington: NASA SP-494, pp. 75–99.

Shemansky, D.E., and Hall D.T. (1992) The distribution of atomic hydrogen in the magnetosphere of Saturn. *J. Geophys. Res. A*, **97**, 41143–61.

Shemansky, D.E., Matheson, P. Hall, D.T. *et al.* (1993) Detection of the hydroxyl radical in the Saturn magnetosphere. *Nature*, **363**, 329–31.

Siscoe, E.C. and Summers, D. (1981) Centrifugally driven diffusion of Iogenic plasma. *J. Geophys. Res. A*, **86**, 8480–4.

Sittler, E.C., Ogilvie, K.W. and Scudder, J.D. (1983) Survey of low-energy plasma electrons in Saturn's magnetosphere: Voyager 1 and 2. *J. Geophys. Res. A*, **88**, 8847–70.

Smith, R.A. and Strobel, D. (1985) Energy partitioning in the Io plasma torus. *J. Geophys. Res. A*, **90**, 9469–93.

Smith, R.A., Bagenal, F., Cheng, A.F. and Strobel, D.F. (1988) On the energy crisis in the Io plasma torus. *Geophys. Res. Lett*, **15**, 545–8.

Smyth, W.H. and Combi, M.R. (1988) A general model for Io's neutral clouds. II Appplication to the sodium cloud. *Astrophys. J.*, **328**, 888–981.

Spencer, J.F. and Schneider, N.M. (1996) Io on the eve of the Galileo mission. *Ann. Rev. Earth Planet Sci.*, **24**, 125–90.

Strobel, D.F. (1989) Energetics, luminosity, and spectroscopy of Io's torus, in *Time Variable Phenomena in the Jovian System* (eds M.J.S. Belton, R.A. West and J. Rahe). Washington: NASA SP-494, pp. 183–94.

Strobel, D.F. and Shemansky D.E. (1982) EUV emission from Titan's upper atmosphere: Voyager 1 encounter. *J. Geophys. Res.*, **87**, 1361–8.

Thomas, N. (1992) Optical observations of Io's neutral clouds and plasma torus. *Surv. Geophys.*, **13**, 91–164.

Thorne, R.M. (1983) Microscopic plasma processes in the Jovian magnetosphere, in *Physics of the Jovian Magnetosphere* (ed. A.J. Dessler). New York: Cambridge University Press, pp. 454–80.

Vasyliunas, V.M. (1986) The convection-dominated magnetosphere of Uranus. *Geophys. Res. Lett.*, **13**, 621–3.

Weiser, H., Vitz, R.C. and Moos, H.W. (1977). Detection of Lyman α emission from the Saturnian disk and from the ring system. *Science*, **127**, 755–7.

Acknowledgements

This article is dedicated to the memory of my friends Bob Smith and Chris Goertz who have contributed so much to our understanding of the physics of planetary tori, and whose lives and careers were brutally cut short a brief year ago.

Cross references

Io
Ionosphere
Magnetospheres of the outer planets
Plasma
Radio astronomy
Radio science
Ulysses mission
Voyager missions

PLANETESIMAL

According to the Chamberlin–Moulton planetesimal hypothesis (q.v.), the 'planetesimals' were identified as solid particles ranging from dust sized (hence 'dust-cloud hypothesis') to meteorite sized. Today, the term planetesimal is usually taken to include asteroids and even larger protoplanetary bodies (Lissauer, 1993). Chamberlin and Moulton (1900) developed the concept of a 'near-miss' encounter between two stars (an idea proposed earlier in 1745 by G.L.L. Buffon, 1707–1788), in which a large tidal protuberance, 'filament', or 'solar nebula' in a flattened disk, was generated from the surface of the major star that was destined to become our Sun. In Buffon's suggestion the collision was between a comet and the star. In the Chamberlin–Moulton model a series of violent eruptions created clouds of hot matter accelerated by the passing star. As the droplets cooled they became solid 'planetesimals' which possessed a high angular momentum. Interparticle collisions began and progressively built up into planet-sized bodies (see Planetary rotation). Stars have now been observed surrounded by what appear to be protoplanetary disks. These appear to consist of a mixture of gas and condensed matter, for which certain meteorites seem to offer the best geochemical model. While the rocky, inner (terrestrial-type) planets seemed to have accumulated in ever-larger pairs of planetesimal to protoplanet dimensions (Wetherill, 1989, 1990; Lissauer 1993), the Jovian planets seem to call for a two-stage growth, culminating in the gravitational capture of their gigantic gas envelopes.

What was the original nature of planetesimals? The Chamberlin–Moulton model of hot droplets is no longer acceptable (Safronov, 1969). The trail seems to lead to the interstellar dust that has been identified and spectroscopically analyzed (Greenberg, 1988). Two types of this dust are recognized: (1) highly diffuse clouds without volatiles like water; and (2) the protosolar nebulae which include dust particles mantled with volatiles of H_2O, CO_2, etc.

Three stages appear (Greenberg and Hage, 1991): (1) a silicate core with an organic refracting mantle (about 0.25 μm in diameter); (2) a 'precometary grain' on which there is a cover of ices, mainly H_2O; and (3) a cluster of the above forming a porous, low-density 'coma grain' (1 μm or more in diameter). In interstellar space the ices of simple chemical compounds are subjected to UV radiation, so-called 'photoprocessing', building up a variety of complex hydrocarbons (and depleting the free oxygen available).

It was postulated by Kuiper in 1951 that there should be a close-in disklike ring of planetesimals somewhere out from Neptune. In this Kuiper belt a very large, asteroid-sized body was identified in 1992 (reported in *Science*, **257**, 1865), some 200 km in diameter, and approximately 1.6×10^9 km beyond Neptune. Short-period comets could originate from this belt. Others appear to be low-volatile fragments of planetoid disruption.

In what is called the 'outer solar system' it seems inevitable that there should be diffusion of planetesimals that did not get caught up in the gravitational sweeping of the circumsolar disk during the accretion stage. Besides the Kuiper disk (at < 500 AU), there is also the Oort cloud (at $< 5 \times 10^4$ AU) which orbits the solar system and seems to be the source of the long-period comets. Stern (1990) postulates that in both of these vast clouds there is a 'substantial population' of asteroids and protoplanetary bodies of the order of 1000 km in diameter.

Slow accretion of planetesimals was necessary in the Earth's formative stages to accommodate the initial cooling required. The Earth's surface has always been cool (at least for the last 4 billion years, as shown by evidence of erosion by running water and sedimentation in bodies of standing, liquid water). All the geochemical components in the present Earth must have been present at the planetesimal stage; as Urey pointed out, volatile elements like bismuth, for example, would have been driven off by any overall melting. Volatile diffusion ('outgassing') has led to the progressive growth of the hydrosphere and atmosphere. Climatically, the Earth has, since about 4 billion years ago, always maintained the same mean surface temperature (about 20 ± 5°C), although the record shows cyclical recurrence of ice ages alternating with long intervals of more benign character. Occasional impacts by planetesimals or small asteroids have never been so catastrophic as to disturb the essential equilibrium required for terrestrial geological and biological evolution.

Rhodes W. Fairbridge

Bibliography

Chamberlin, T.C. (1900) An attempt to test the nebular hypothesis by the relations of masses and momenta. *J. Geol.*, **8**, 58–73. (See also *Astrophys. J.*, **14**, 17, 1901)
Chamberlin, T.C. (1927) *The Origin of the Earth*. Chicago: Chicago University Press.
Chamberlin, T.C. and Moulton, F.R. (1900) Certain recent attempts to test the nebular hypothesis. *Science*. (n.s.), **12**, 201–8.
Fairchild, H.L. (1904) Geology under the planetesimal hypothesis. *Geol. Soc. Am. Bull.*, **15**, 243–66.
Gold, T. (1963) Problems requiring solution, in: *Origin of the Solar System* (eds R. Jastrow and A.G.W. Cameron), New York: Academic Press, pp. 171–4.
Goldreich, P. and Ward, W.R. (1973) Formation of planetesimals. *Astrophys. J.*, **183**, 1051–61.
Greenberg, J.M. (1988) in *Dust in the Universe*. (eds M. Bailey and D.A. Williams. Cambridge University Press, pp. 121–00.
Greenberg, J.M., and Hage, J.I. (1990) *Astrophys. J.*, **361**, 260–74.
Jeffreys, H. (1924) *The Earth*. Cambridge University Press (and subsequent editions).
Lissauer, J.J. (1993) Planet formation. *Ann. Rev. Astron. Astrophys.*, **31**, 129–74.
Safronov, V.S. (1969) *Evolution of the Protoplanetary Cloud and Planets*. Moscow: Nauka Press (in Russian English translation by NASA, TTF-677, 1972). (See also *Icarus*, **94**, 260–71, 1991)
Stern, S.A. (1991) On the number of planets in the outer solar system: evidence of a substantial population of 1000-km bodies. *Icarus*, **90**, 271–81.
ter Haar, D. and Cameron, A.G.W. (1967) Solar system: review of theories, in *The Encyclopedia of Atmospheric Sciences and Astrogeology* (ed. R.W. Fairbridge). New York: Reinhold Publishing Co., 890–9.
Tonks, W.B. and Melosh, H.J. (1992) Core formation by giant impacts. *Icarus*, **100**, 326–46.
Urey, H.C. (1952) *The Planets, their Origin and Development*. New Haven: Yale University, Press.
Urey, H.C. (1959) Primary and secondary objects. *J. Geophys. Res.*, **64**, 1721–37.
Wetherill, G.W. (1990) *Ann. Rev. Earth Planet. Sci.*, **18**, 205–56.

Acknowledgements

This manuscript was kindly reviewed by J. Mayo Greenberg, Leiden; an early draft was kindly reviewed by Jack Lissauer.

Cross references

Chamberlin, Thomas Chrowder
Dust

PLASMA

A plasma is comprised of discrete electrically charged particles which are coupled through the long-range Coulomb potential so that they behave collectively. For a plasma system to exhibit this collective behavior (rather than each particle being unaffected by other charges) it must contain a sufficiently large number of particles. Formally, there must be a large number of particles within a sphere with radius equal to a Debye length, the scale length for the electrostatic screening potential,

$$\lambda_D = (kT_e\epsilon_o/n_e q_e^2)^{1/2}$$

where T_e, q_e are n_e are the electron temperature, charge and density; k is the Boltzmann constant; ϵ_o is the dielectric constant in free space. Thus the condition that particles behave collectively as a plasma is $N_D = \frac{4}{3}\pi\lambda^3_D \gg 1$. On scale lengths larger than a Debye length, the plasma is electrically neutral when the number density of positive ions is on average equal to the electron number density.

The simplest plasma consists of electrons and one species of ions, protons (H^+), for example. More complex plasmas include several different ion species, neutral atoms and molecules. Solar system plasmas can be categorized by their sources: the solar wind, ionospheres, magnetospheres and comets. The solar wind is comprised of electrons and protons (the ionized part of the Sun's hydrogen atmosphere) which have sufficient energy to escape the Sun's gravity. Solar radiation photoionizes neutral atoms and molecules in planetary atmospheres to form, in most cases, an ionosphere with ion species reflecting the composition of the neutral atmosphere, mainly H^+ in the case of the giant planets and O^+, O_2^+ and NO^+ in the case of the Earth. An ionosphere can be simply described as a layer of ionization where the rate of photoionization balances the rate of recombination of the electrons and ions. Below the ionosphere layer, where the densities are higher, the recombination rate is higher and fewer ionizing photons penetrate. Above this layer the neutral densities and hence the source of particles for ionization, decrease. Magnetospheric plasmas, controlled by planetary magnetic fields, can have several sources which we discuss below. As a comet moves on its eccentric orbit towards the inner solar system, the escaping neutral gases form a very large cloud which is ionized by solar photons (and by solar wind impact) to form a very extended plasma tail of electrons and CO^+, H_2O^+ and OH^+ ions (see Comet).

In hot, tenuous plasmas collisions between particles are very rare, so that the plasma is primarily affected by electric and magnetic fields. In cold, dense plasmas collisions become important; one also has to consider ionization, charge exchange and recombination processes. While one expects cold, dense, collision-dominated plasmas to be in thermal equilibrium, even hot, tenuous plasmas in space are generally found not far from equilibrium, i.e. their particle distribution functions are observed to be approximately Maxwellian (though the ion and electron populations often have different temperatures). This fact is remarkable considering that the source mechanisms tend to produce particles with an initially very narrow range in energy, and timescales for equilibration by means of Coulomb collisions are usually much longer than transport timescales. At the same time, space plasmas support a variety of plasma waves which have various energy sources and cover a wide range of frequencies. Interactions between these waves and particle populations are thought to be responsible for bringing the bulk of the plasma towards thermal equilibrium as well as accelerating or scattering particles at higher energies. In addition to the thermal populations (which make up the bulk of the plasma by number density), all planetary magnetospheres contain populations of energetic particles which often dominate the energy density (Priest, 1985; Parks, 1991).

Plasma measurements

The most direct method of measuring the properties of plasmas in space is by placing a plasma detector on a spacecraft which flies through the plasma. By making the electric potential of a detector positive or negative, electrons or ions are correspondingly attracted or repelled. The electric potentials of a series of grids or metal surfaces are designed so that charged particles are guided through the instrument selecting only particles within a specific range of energy per unit charge (E/Q) (see Thermal plasma instrumentation). By varying the potentials, the spectrum of the particles' E/Q can be measured, ranging from a few volts to tens of kilovolts. If all the charged particles are of the same known species (e.g. electrons, protons), the E/Q spectrum is a direct measure of the velocity distribution of the particles. By pointing detectors in different directions, full three-dimensional velocity distributions can be measured in seconds. The velocity distributions of different ionic species can be measured with an electrostatic instrument if their spectral peaks are well separated in E/Q. Unfortunately, there are many space plasmas where the dominant species have the same or similar mass per charge ratios (e.g. O^+ and S^{++} in Jupiter's magnetosphere, or water dissociation products H_2O^+, OH^+, etc.) such that their E/Q spectra overlap. To separate these ion species it is necessary to add a deflecting magnet to the electrostatic analyzer, or to measure the time each particle takes to traverse a chamber in the instrument (Young, 1989; Young *et al.*, 1989; Bame *et al.* 1989)

While plasma detectors provide detailed information about the particles' velocity distribution, from which bulk parameters such as density, temperature and flow velocity are derived, the plasma properties are only measured in the vicinity of the spacecraft. With the few existing spacecraft it is impossible to measure the changing properties of the many different plasmas in the solar system. Some of the most interesting space plasmas, however, can be remotely monitored by observing emissions of electromagnetic radiation. Dense plasmas, such as Jupiter's plasma torus, comet tails, Venus' ionosphere and the solar corona, have collisionally excited line emissions at optical or UV wavelengths. Similarly, when magnetospheric particles bombard the planets' polar atmospheres, various auroral emissions are generated from radio to x-ray wavelengths. Thus our knowledge of space plasmas is based on combining the remote sensing of plasma phenomena with spacecraft measurements which provide 'ground truth' details of the particles' velocity distribution as well as the local electric and magnetic fields that may be interacting with the plasma.

Obstacles in a flowing plasma

By the time plasma from the Sun reaches the planets its kinetic energy is largely bulk motion (i.e. the flow is supersonic) and, as the interplanetary magnetic field (IMF) is weak, the solar wind is super-Alfvénic (i.e. the solar wind speed is greater than the speed of Alfvén waves, magnetohydrodynamic waves that can propagate in a magnetized, collisionless medium). The fact that the solar wind is supersonic means that generally there is a bow shock upstream of the obstacle. The plasma is slowed down and heated as it passes through the shock and hence the flow around the obstacle is then sub- or trans-sonic. In contrast to the solar wind, plasma flows in planetary magnetospheres span wide ranges of sonic and Alfvénic Mach numbers, a consideration that must be kept in mind when comparing plasma interactions of different planetary satellites (e.g. the sonic/Alfvén Mach numbers for the flow near Io, Titan and Triton are 2/0.15, 0.6/2 and 1/0.2 respectively; Neubauer, Luttgen and Ness, 1991).

With regard to the characteristics of the obstacle, it is convenient to consider first the two extreme situations where the object is taken to be either a perfect insulator or a perfect conductor. It is then necessary to consider the effects of finite conductivity, since planetary bodies have effective conductivity in a range between these two extremes.

Non-conducting object

A magnetic field diffuses through an object with a time scale $\tau_d \sim \mu_o\sigma L^2$, where L is the size and σ the electrical conductivity of the body. If this diffusive timescale is much less than the timescale for changes in the ambient magnetic field, the field passes through the body largely unperturbed. For a magnetic field 'frozen' into a plasma flowing at a characteristic speed V the object sees the field change over the convective timescale $\tau_c \sim L/V$. Hence the magnetic interaction is weak for a non-conducting body with low magnetic Reynolds number ($R_m = \tau_d/\tau_c = \mu_o\,\sigma LV \ll 1$).

Although the magnetic field readily diffuses through the non-conducting body, the plasma particles obviously cannot penetrate the body and are therefore absorbed. Because the flowing plasma is absorbed on the upstream surface there is a cavity behind the object and a wake is formed downstream as the plasma expands into the low-pressure region (Figure P23a). The Earth's Moon and most of the icy satellites of the outer planets are non-conductors and hence simple absorbers of the flowing plasma in which they are embedded.

Perfectly conducting object

When there is a relative motion V' between a magnetized plasma and a conducting body the Lorentz electric field $E = -V' \times B$ drives a current $J = \sigma E$ in the object (Figure 23b). The current in the body in turn produces a perturbation in the background magnetic field. Since the magnetized plasma is highly anisotropic (with parallel conductivity $\sigma_{\parallel} \gg \sigma_{\perp}$) the current is carried away from the flanks of the object along the magnetic field. In the magnetohydrodynamic (MHD) regime the plasma is coupled to the magnetic field and hence the plasma flow is also perturbed by the conducting body. In the case of a perfect conductor (i.e. $R_m \gg 1$) the resulting motion of the plasma in the tube of magnetic flux that intersects the body exactly matches the motion of the conductor. The surrounding plasma is then deflected around the body in a manner similar to incompressible hydrodynamic flow around a cylinder with essentially no wake downstream. The perturbations in the magnetic field (b) and the plasma flow (v) are an Alfvénic disturbance, which propagates along the ambient magnetic field with a characteristic speed of

$$V_A = B/(\mu_o \rho)^{1/2}$$

and satisfies the Alfvén relation $v/V_A = \pm b/B$ (where the sign corresponds to propagation parallel or antiparallel to the ambient magnetic field). One can consider these Alfvén waves to be carrying field-aligned currents that complete the electrical circuit that flows through the object. If the object has a substantial ionosphere (with a conductance on the order of 1 mho), such as in the cases of Venus, Mars, Titan and Io, these currents flow through the ionosphere rather than the solid object. To first order, Jupiter's moon Io can be

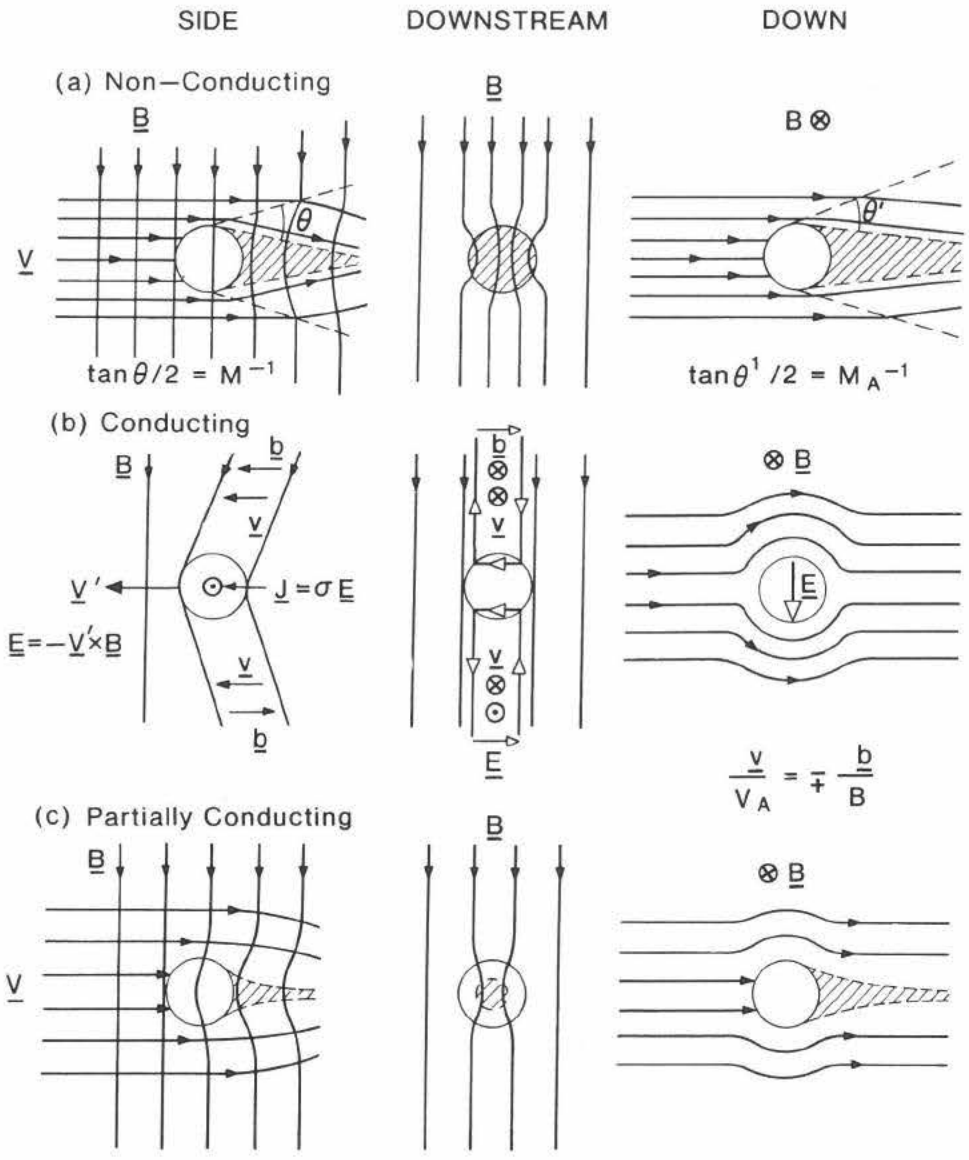

Figure P23 The interaction of magnetized plasma with an object that is (a) non-conducting; (b) conducting; and (c) partially conducting. The hatching indicates the region of low density in the object's wake. (The magnetic field $\boldsymbol{B}$, the solar wind flow $\boldsymbol{V}$, the motional electric field $\boldsymbol{E}$ and the induced current $\boldsymbol{J}$ are given by arrows. The symbols ⊗ and ⊙ indicate arrows pointing into and out of the figure respectively. The perturbations in flow and magnetic field are shown by v and b)

described as a conducting object embedded in magnetospheric plasma flow (Belcher, 1987).

Partially conducting object

When the object has a finite conductivity the flow perturbation is insufficient to deflect the surrounding plasma to flow around the body and hence some is absorbed (Figure P23c). The plasma flow is reduced near the object and the magnetic field being 'hung up' in the stagnant flow. Since the magnetic field far from the object continues to be convected in the unperturbed flow the magnetic field lines become bent or 'draped' over the object to form a magnetic tail or wake downstream.

Object with an atmosphere

On the dayside of all objects having an atmosphere, the Sun's ultraviolet emissions ionize some of the neutral atoms. For objects that are embedded in a magnetospheric plasma (e.g. Titan, Triton and Io), ionization by particle impact may also be significant. In any case, the degree of ionization determines the conductivity of the upper atmosphere (ionosphere) and thus affects the nature of the interaction of the object with the plasma in which it is immersed. In the case of a planet with a dense ionosphere ($\sigma \rightarrow \infty$ or effectively $\sigma > \sim 1$ mho) the solar wind magnetic field is excluded and the flow is diverted around the flanks of the body (the case at Mars and Venus, to first order). Similar situations are found at Titan, Triton and Io, except that there is no bow shock for the sub- or trans-sonic magnetospheric flows. The boundary between the ionosphere and the surrounding plasma, the ionopause, is located where the combined magnetic and ram pressure of the external plasma is balanced by the particle pressure (P) in the ionosphere (Figure P24a). When the ionization is weak ($\sigma \rightarrow 0$) the magnetic field and plasma flow are dragged through the resistive ionosphere, causing a substantial downstream wake.

We must further consider the consequences of the ionization of any neutral material extending out into the streaming plasma. On ionization the particle 'sees' the Lorentz electric field and is accelerated up to the ambient flow. The momentum gained by the newly created ions comes from the surrounding plasma which correspondingly loses momentum. This effect is called 'mass loading' and contributes to the local deceleration of the flow and the draping of field lines over an object with a substantial atmosphere (e.g. comets, Venus and Titan; Luhmann, 1986; Luhmann *et al.*, 1992; Cheng and Johnson, 1989.)

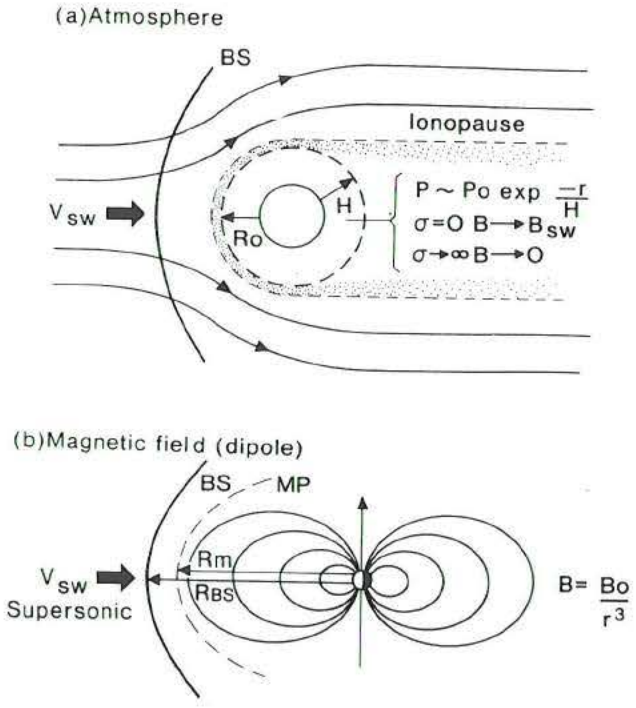

Figure P24 The interaction of a flowing magnetized plasma (V_{SW}) with an object possessing (a) an atmosphere of surface pressure P_0 and scale height H; (b) a magnetic field. The bow shock (BS) and magnetopause (MP) are shown.

Magnetized object

Well before Biermann (1957) provided cometary evidence of a persistent solar wind, Chapman and Ferraro (1931) considered how a strongly magnetized body would deflect a flow of particles from the Sun and made an estimate of the location of the magnetopause stagnation point – the boundary between the magnetosphere in the direction of the Sun. They proposed that a dipolar magnetic field (of strength B_o at the planet's equatorial radius R_p) would 'stand off' the flow to a distance R_{CF}, where the external ram pressure of the solar wind balances the internal pressure of the planet's magnetic field (Figure 24b):

$$R_{CF} / R_p = \zeta \, (B_o^2 / 2 \, \mu_o \, \rho_{sw} \, V_{sw}^2)^{1/6} \qquad \text{(P8)}$$

where ρ_{sw} and V_{sw} are the ion mass, density and flow speed of the solar wind. The dimensionless factor $\zeta \sim 1.3$ corrects for the various oversimplifications in the above description (Siscoe, 1979). The observed magnetopause stand-off distances, R_m, are found to be compatible with the values R_{CF} calculated using observed upstream conditions (see Table P8) except in the case of Jupiter where R_m is observed to be highly variable with an average value about twice the nominal value, owing to the presence of interior plasma with a pressure comparable to the magnetic field pressure.

The term magnetosphere was coined by Gold (1959) to describe the region of space wherein the principal forces on a plasma are electrodynamic in nature and are a result of the planet's magnetic field.

Plasma sources

The main source of plasma in the solar system is clearly the Sun. The solar corona, the upper atmosphere of the Sun (which has been heated by some, as yet undetermined, process to temperatures of 1–2 million K), streams away from the Sun at a more or less steady rate of 10^9 kg s^{-1} in equal numbers (8×10^{35} s^{-1}) of electrons and ions. Magnetospheres contain considerable amounts of plasma from various sources (Figure P25). Table P9 describes the primary and secondary sources of plasma for the six planetary magnetospheres.

First, the magnetopause is not entirely plasma-tight. Whenever the IMF has a component antiparallel to the planetary magnetic field, magnetic reconnection is likely to occur and solar wind plasma will leak into the magnetosphere across the magnetopause. Solar wind material is identified in the magnetosphere by its energy and characteristic composition of protons (H^+) with $\sim$ 4% alpha particles (He^{++}) and trace heavy ions.

Second, although ionospheric plasma is generally cold and gravitationally bound to the planet, a small fraction has sufficient energy to escape up magnetic field lines and into the magnetosphere. Ionospheric plasma has a composition that reflects the composition of the planet's atmosphere (e.g. O^+ for the Earth, H^+ for the outer planets).

Third, the interaction of magnetospheric plasma with any natural satellites that are embedded in the magnetosphere can generate significant quantities of plasma. The ionization of the outermost layers of a satellite atmosphere by the impacting plasma flow can be a major source of plasma (nearly 1 metric ton per second in the case of Io). Energetic particle sputtering of the satellite surface or atmosphere produces less energetic ions directly, or an extensive cloud of neutral atoms which are eventually ionized far from the satellite. The distributed sources of water-product ions (totaling $\sim$ 2 kg s^{-1}) in the magnetosphere of Saturn suggest that energetic particle sputtering of the icy satellites, particularly Rhea, Dione and Tethys, is an important process. Although the sputtering process, which removes at most a few microns of surface ice per thousand years, is probably insignificant in geological terms, sputtering has important consequences for the optical properties of the surface (Cheng and Johnson, 1989).

Plasma flows

Magnetospheric configuration is generally well described by magnetohydrodynamic theory (MHD) in which the magnetic field can be

Table P8 Properties of the solar wind and planetary magnetic fields

	Mercury	Earth	Jupiter[a]	Saturn[a]	Uranus[a]	Neptune[a]
Distance, a_{planet} (AU)	0.31–0.47	1[b]	5.2	9.5	19	30
Solar wind density (cm^{-3})	35–80	8	0.3	0.1	0.02	0.008
Radius, R_{Planet} (km)	2439	6373	71 398	60 330	25 559	24 764
Magnetic moment/M_{Earth}	4×10^{-4}	1[c]	20 000	600	50	25
Surface magnetic field B_0 (gauss)	3×10^{-3}	0.31	4.28	0.22	0.23	0.14
R_{CF}[d]	1.4–1.6 R_M	10 R_E	42 R_J	19 R_S	25 R_U	24 R_N
Observed size of magnetosphere	1.4 R_M	8–12 R_E	50–100 R_J	16–22 R_S	18 R_U	23–26 R_N

[a] Magnetic field characteristics from Acuña and Ness (1976), Connerney, (1987, 1991).
[b] 1 AU = 1.5×10^8 km.
[c] $M_{Earth} = 7.906 \times 10^{25}$ gauss $cm^3 = 7.906 \times 10^{15}$ T m^3.
[d] R_{CF} is calculated using equation (P8) for typical solar wind conditions of $\rho_{sw} \sim (8 \text{ amu cm}^{-3})/a^2_{planet}$ and $V_{sw} \sim 400$ km s^{-1}.

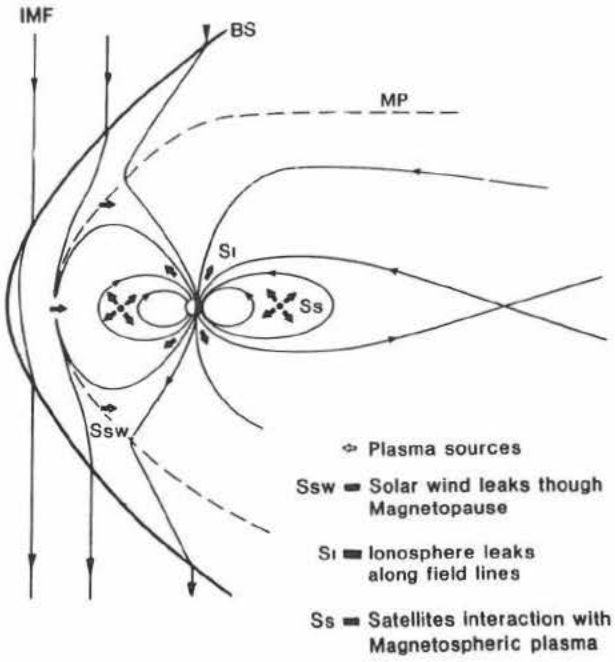

Figure P25 Sources of magnetospheric plasma.

considered to be frozen into the plasma flow. Thus we need to consider the processes controlling magnetospheric flows. The two largest sources of momentum in planetary magnetospheres are the planet's rotation and the solar wind. The nature of any large-scale circulation of material in the magnetosphere depends on which momentum source is tapped. For planetary magnetospheres, corotation of plasma with the planet is a useful first approximation, with any departures from strict corotation occurring when certain conditions break down. It may be helpful to think of plasma in the magnetosphere as mass that is coupled by means of magnetic field lines to a giant flywheel (the planet) with the ionosphere acting as the clutch.

Corotation

For magnetospheric plasma to rotate with the planet, the first two conditions are that the upper region of the neutral atmosphere must corotate with the planet and must be closely coupled to the ionosphere by collisions. The electrical conductivity of the ionosphere σ^i is large so that in a corotating ionosphere (with velocity V^i) any horizontal currents (perpendicular to the local magnetic field) are given by Ohm's law,

$$J_{\perp}{}^i = \sigma^i (E^i + V^i \times B)$$

Just above the ionosphere the conductivity perpendicular to the magnetic field in the (collision-free) magnetosphere, $\sigma_{\perp}{}^m$, is essentially zero and because the plasma particles are far more mobile in the direction of the local magnetic field, the parallel conductivity $\sigma_{\parallel}{}^m$ is large. Therefore, magnetic field lines can be considered to be equipotentials ($E \cdot B = 0$) in the magnetosphere and the electric field in the magnetosphere ($E^m = -V^m \times B$) can be mapped into the ionosphere (Figure P26a). Because the ionosphere is relatively thin, the electric field E^m just above the ionosphere is the same as E^i so that we can write

$$J_{\perp}{}^i = \sigma^i (V^i - V^m) \times B$$

The condition for corotation of the magnetospheric plasma is that the ratio J^i/σ^i is sufficiently small that

$$V^m = V^i = \Omega \times r$$

For a dipolar magnetic field that is aligned with the rotation axis, the corotational electric field (in the equatorial plane) is therefore radial with magnitude $E_{co} = \Omega B_o/r^2$.

It is clear that large ionospheric conductivities facilitate corotation. The large $\sigma_{\parallel}{}^m$ also means that any currents in the magnetosphere that result from mechanical stresses on the plasma are directly coupled by field-aligned currents to the ionosphere. Thus corotation breaks down when mechanical stresses on the magnetospheric plasma drive ionospheric currents which are sufficiently large that the ratio J^i/σ^i becomes significant. Such conditions might occur in regions of the magnetosphere where there are large increases in mass density due to local ionization of neutral material, where there are strong radial motions of the plasma or where there are sharp gradients in plasma pressure. When the magnetosphere imposes too large a load, the ionospheric clutch begins to slip.

Solar wind convection

Next let us consider how the momentum of the solar wind may be harnessed by processes occurring near the magnetopause where the external interplanetary magnetic field (B_{IMF}) interconnects with the planetary magnetic field. Figure P26b shows that at the poles the planetary magnetic field lines are open to the solar wind. The solar wind drives a plasma flow across the polar caps and the field lines from the polar region move in the direction of the solar wind flow, being pulled by the solar wind over the poles and back into the extended magnetotail. Conservation of flux requires that field lines are further cut and reconnected in the tail.

The MHD condition of the field being frozen to the flow can be written as $E + V \times B = 0$ which allows the convection electric field to be written

$$E_{cv} = -\eta V_{sw} \times B_{IMF}$$

where η is the efficiency of the reconnection process in harnessing the solar wind momentum, ~ 0.1 for the Earth. In simple magnetospheric models E_{cv} is assumed constant throughout the magnetosphere. The corresponding circulation is given by the $E \times B$ drift,

$$V_{cv} = \eta V_{sw} (B_{IMF}/B_o) (r/R_p)^3$$

After being carried tailward at high latitudes, the plasma then drifts towards the equatorial plane and eventually returns in a sunward flow to the dayside magnetopause.

Comparison of the corresponding electric fields indicates whether the magnetospheric circulation is driven primarily by the solar wind

Table P9 Plasma characteristics of planetary magnetospheres

	Mercury	Earth	Jupiter	Saturn	Uranus	Neptune
Maximum density (cm^{-3})	1	1–4000	>3000	~100	3	2
Primary sources	H^+ Solar wind	O^+, H^+ Ionosphere[a]	O^{n+}, S^{n+} Io	O^+, H_2O^+, H^+ Dione, Tethys	H^+ Ionosphere	N^+, H^+ Triton
Secondary sources	?	H^+ Solar wind	H Ionosphere	N^+, H^+ Titan	H^+ Solar wind	H^+ Solar wind
Source strength (ions s^{-1})	?	2×10^{26}	$>10^{28}$	10^{26}	10^{25}	10^{25}
(kg s^{-1})		5	700	2	0.02	0.2
Lifetime	Minutes	Days[a], hours[b]	10–100 days	30 days to years	1–30 days	~1 day
Plasma motion	Solar wind driven	Rotation[a], solar wind[b]	Rotation	Rotation	Solar wind + rotation	Rotation (+ solar wind?)

[a] Inside plasmasphere.
[b] Outside plasmasphere.

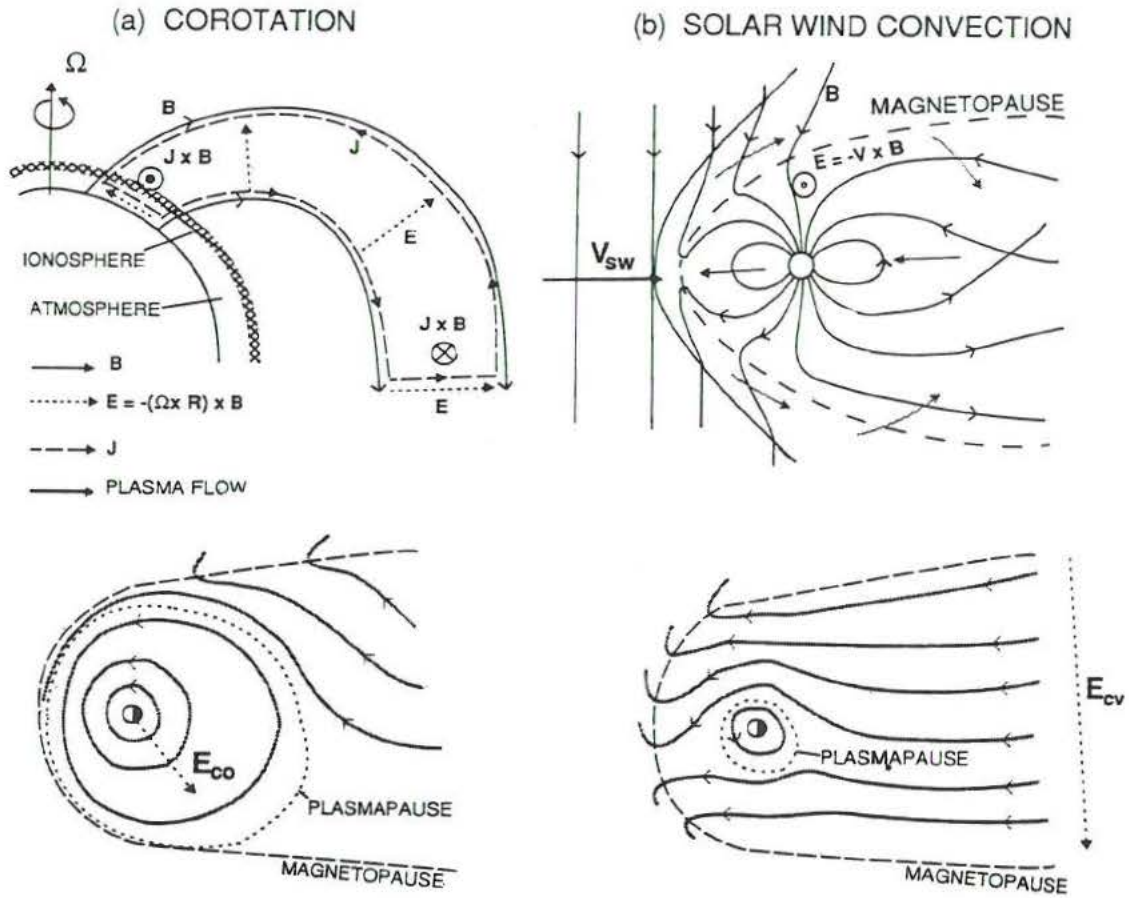

Figure P26 Large-scale magnetospheric circulation driven by (a) planetary rotation; (b) the solar wind. (The magnetic field ***B***, the solar wind flow ***V***, the motional electric field ***E*** and the induced current ***J*** are given by arrows. Ω labels the planet's spin axis. The symbols ⊗ and ⊙ indicate arrows pointing into and out of the figure respectively).

or by the planet's rotation. Since E_{co} is proportional to R^{-2} and E_{cv} is constant, it seems reasonable to expect that corotation dominates close to the planet while solar wind driven convection dominates outside a critical distance.

$$R_c = (\Omega B_o/\eta\, V_{sw}\, B_{IMF})^{1/2}$$

This simply says that magnetospheres of rapidly rotating planets with strong magnetic fields are dominated by rotation while the solar wind controls the plasma flow in smaller magnetospheres of slowly rotating planets (Dessler, 1983; Hill and Dessler, 1991; Parks, 1991).

Plasma loss processes

For the planets with plasma transport driven by the solar wind, magnetospheric plasma is removed and carried away in the solar wind quite rapidly, on timescales of minutes (in the case of Mercury) to several days (in the case of Uranus). In rotation dominated magnetospheres radial transport of plasma is slow so that high plasma densities build up (Table P9) and other loss mechanisms can be significant. In particular, charge exchange occurs between corotating ions and neutral material (e.g. sputtered neutral clouds around

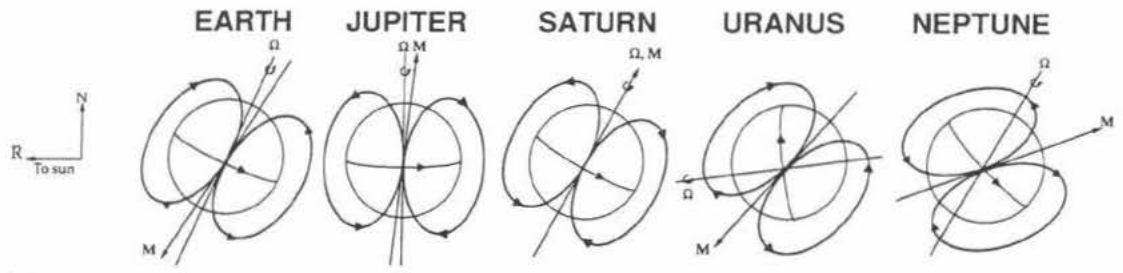

	EARTH	JUPITER	SATURN	URANUS	NEPTUNE
Obliquity $\cos^{-1}(\Omega \cdot N)$ =	23.5°	3.1°	26.7°	97.9°	29.6°
Dipole Tilt $\cos^{-1}(\Omega \cdot M)$ =	+11.7°	-9.6°	-0.0°	-59°	-47°
Solar Wind Angle $\cos^{-1}(\Omega \cdot R)$ =	66.5 - 113.5°	86.9 - 93.1°	63.7 - 116.5°	7.9 - 172.1°	60.4 - 119.6°

Figure P27 Orientations of the planets and their magnetic fields.

satellites and rings, or the extended neutral atmospheres of the giant planets). As a result of the charge-exchange process the corotating ion becomes neutralized so that it is no longer confined by the planet's magnetic field. The neutralized ion has maintained most of its corotational momentum and hence escapes from the planet. Such a wind of escaping fast neutral sodium atoms has been observed extending to several hundred Jovian radii (Mendillo *et al.*, 1990). Charge exchange is also a dominant loss process in the magnetosphere of Saturn (Cheng and Johnson, 1989).

Plasma properties at the planets

Solar wind plasma

The solar wind is the outward expansion of the solar corona (Van Allen, 1990; Pizzo, Holzer and Sime, 1988; Marsch and Schwenn, 1992). At Earth's orbit and beyond, the solar wind has an average speed of about 400 km s^{-1}. The density of particles (mainly electrons and protons) is observed to decrease, from values of about 3–10 cm^{-3} at the Earth as the inverse square of the distance from the Sun, consistent with a steady radial expansion of the solar gas into a spherical volume, reaching values of 0.005 cm^{-3} at Neptune (Table P8).

The solar wind speed, while varying between about 300 and 700 km s^{-1}, always greatly exceeds the speed of waves characteristic of a low density, magnetized and completely ionized gas (MHD or Alfvén waves). Thus a shock is formed upstream of an obstacle (such as a planetary magnetosphere) that is imposed on the super-Alfvénic solar wind flow. A planetary bow shock can be described in fluid terms as a discontinuity in bulk parameters of the solar wind plasma in which mass, momentum and energy are conserved. Entropy, however, increases as the flow traverses the shock, with the solar wind plasma being decelerated and heated so that the flow can be deflected around the magnetosphere (see Shock wave). Thus a shock requires dissipative processes and the presence of a magnetic field allows dissipation to occur on a scale much smaller than a collisional scale length. Although planetary bow shocks do not play a significant role in magnetospheric processes, the crossings of spacecraft through planetary bow shocks have provided an opportunity to study the exotic plasma physics of high Mach number collisionless shocks that cannot be produced in a laboratory (Russell, Hoppe and Livesey, 1982; Slavin *et al.*, 1985; Bagenal *et al.*, 1987; Moses *et al.*, 1990).

Magnetospheric plasmas

Spacecraft have explored the plasma environments of all the planets except Pluto. With the exception of Venus and Mars, all these planets have significant magnetic fields and magnetospheres. In the cases of Venus and Mars the solar wind interaction with ionospheres is confined to a small region close to the planet where the solar wind plasma is deflected around the planet, picking up O^+ ions from the upper layers of the planet's atmosphere (Luhmann, 1986; Luhmann *et al.*, 1992). Given the roughly constant solar wind speed, the size of a planet's magnetosphere (R_{CF}) depends only on the ambient solar wind density and the planet's magnetic field [see equation (P8)]. Thus we expect a planet with a strong magnetic field to have a large magnetosphere, and even the weak fields of Uranus and Neptune produce moderate-sized magnetospheres in the tenuous solar wind of the outer solar system (see Magnetospheres of the outer planets). Table P8 shows that the measured sizes of planetary magnetospheres generally agree quite well with the theoretical R_{CF} values. Jupiter is the only notable exception, where the plasma pressure inside the magnetosphere is sufficient to 'inflate' further the magnetosphere. This makes the magnetosphere of Jupiter a huge object – about 1000 times the volume of the Sun, with a tail that extends at least 6 AU in the direction away from the Sun, beyond the orbit of Saturn. If the Jovian magnetosphere were visible from Earth, its angular size would be twice that of the Sun, even though it is at least four times farther away. The magnetospheres of the other giant planets are much more modest (while still dwarfing that of the Earth), having a similar scale of about 20 times the planetary radius, comparable to the size of the Sun. With only a weak magnetic field and being embedded in the denser solar wind close to the Sun, Mercury has a very small magnetosphere (Russell, Baker and Slavin, 1988; see Mercury: magnetic field and magnetosphere).

While the size of a planetary magnetosphere depends on the strength of a planet's magnetic field, the configuration and internal dynamics depend on the field orientation (illustrated in Figure P26) which is described by two angles: the tilt of the magnetic field with respect to the planet's spin axis and the angle between the planet's spin axis and the solar wind direction (which is generally within a few degrees of being radially outward from the Sun). Since the direction of the spin axis with respect to the solar wind direction only varies over a planetary year (many Earth years for the outer planets), and the planet's magnetic field is assumed to vary only on geological timescales, these two angles are constant for the purposes of describing the magnetospheric configuration at a particular epoch. Earth, Jupiter and Saturn have both small dipole tilts and small obliquities. This means that the orientation of the magnetic field with respect to the solar wind does not vary appreciably over a planetary rotation period and that seasonal effects are small. Thus Earth, Jupiter and Saturn have symmetric and quasi-stationary magnetospheres, with Earth and Jupiter each exhibiting only a small wobble due to their ~ 10° dipole tilts. In contrast, the large dipole tilt angles of Uranus and Neptune mean that the orientation of their magnetic fields with respect to the interplanetary medium varies considerably over a planetary rotation period, resulting in highly asymmetric and time-variable magnetospheres. Furthermore, Uranus' large obliquity means that the configuration of its magnetosphere will have strong seasonal changes over its 84-year orbit.

Table P9 summarizes the basic characteristics of plasmas measured in the magnetospheres of the planets which have detectable magnetic fields. The composition of the ionic species indicates the sources of magnetospheric plasma: satellites in the cases of Jupiter, Saturn and Neptune; the planet's ionosphere in the cases of Earth and Uranus. In the magnetospheres where plasma motions are driven by the solar

wind, solar wind plasma enters the magnetosphere, becoming the primary source of plasma in the case of Mercury's small magnetosphere and secondary plasma sources at Earth, Uranus and Neptune. In the magnetospheres where plasma flows are dominated by the planet's rotation (Jupiter, Saturn and within the Earth's plasmasphere), the plasma is confined by the planet's strong magnetic field for many days so that substantial densities are accumulated.

Thus we can identify three categories of planetary magnetospheres:

1. the large, symmetric and rotation-dominated magnetospheres of Jupiter and Saturn;
2. the small magnetosphere of Mercury where the only source of plasma is the solar wind which drives rapid circulation of material through the magnetosphere; and
3. the moderate-sized and highly asymmetric magnetospheres of Uranus and Neptune, whose constantly changing configuration does not allow substantial densities of plasma to build up. The Earth's magnetosphere is an interesting hybrid of the first two types, with a dense corotating plasmasphere close to the planet and tenuous plasma, circulated by the solar wind driven convection, in the outer region (Bagenal, 1992; Russell, Baker and Slavin, 1988; Parks, 1990).

Fran Bagenal

Bibliography

Acuna, M.H., Ness, N.F. (1976) The main magnetic field of Jupiter. *J. Geophys. Res.*, **81**, 2917–22.

Bagenal, F. (1992) Giant planet magnetospheres. *Ann. Rev. Earth Planet. Sci.*, **20**, 289.

Bagenal, F., Belcher, J.W., Sittler, E.C. and Lepping, R.P. (1987) The Uranian bow shock: Voyager 2 inbound observations of a high Mach number shock. *J. Geophys. Res.*, **92**, 8603–12.

Bame, S.J., Martin, R.H., Comas D.J. *et al.* (1989) Three-dimensional plasma measurements from three-axis stabilized spacecraft, in *Solar System Plasma Physics* (eds J.H. Waite, J.L. Burch and R.L. Moore). American Geophysical Union Publications.

Belcher, J.W. (1987) The Jupiter–Io connection: an Alfven engine in space, *Science*, **238**, 170.

Biermann, L. (1957) Solar corpuscular radiation and the interplanetary gas. *Observatory*, **77**, 109.

Cheng, A.F., Johnson, R.E. (1989) Effects of magnetosphere interactions on origin and evolution of atmospheres, in *Origin and Evolution of Planetary and Satellite Atmospheres* (eds S.K. Atreya, J.B. Pollack and M.S. Matthews) Tucson: University of Arizona Press.

Chapman, S. and Ferraro, V.C.A. 1931. A new theory of magnetic storms. *Terr. Magn. Atmos. Elect.*, **36**, 77–97.

Connerney, J.E.P. (1987) The magnetospheres of Jupiter, Saturn, and Uranus. *J. Geophys. Res.*, **25**, 615–38.

Connerney, J.E.P., Acuña, M.H. and Ness, N.F. (1991) The magnetic field of Neptune. *J. Geophys. Res.*, **96**, 19023.

Dessler, A.J. (ed.) (1983) *Physics of the Jovian Magnetosphere*. Cambridge University Press.

Gold, T. (1959) *Symposium on the Exploration of Space* **64**, pp. 1665–1674

Hill, T.W. and Dessler, A.J. (1991) Plasma motions in planetary magnetospheres. *Science*, **252**, 410–415.

Luhmann, J.G. (1986) The solar wind interaction with Venus. *Space Sci. Rev.*, **44**, 241.

Luhmann, J.G., Russell, C.T., Brace L.H. and Vaisberg, O.L. (1992) The intrinsic magnetic field and solar wind interaction of Mars, in *Mars* (eds H.H. Kieffer, B.M. Jakosky, C.W. Snyder and M.S. Matthews). Tucson: University of Arizona Press.

Marsch, E. and Schwenn, R. (eds) (1992) *Solar Wind Seven*. Pergamon Press.

Mendillo, M., Baumgardner, J., Flynn, B. and Hughes, J. (1990) The extended sodium nebula of Jupiter. *Nature*, **348**, 312–4

Moses, S.L., Coroniti, F.V., Kennel, C.F. *et al.* (1990). Comparison of plasma wave measurements in the bow shocks at Earth, Jupiter, Saturn, Uranus, and Neptune. *Geophys. Res. Lett.*, **17**, 1653–6.

Neubauer, F.M., Luttgen, A. and Ness, N.F. (1991). On the lack of a magnetic signature of Triton's magnetospheric interaction on the Voyager 2 flyby trajectory. *J. Geophys. Res.*, **96**, 19171–5.

Pizzo, V.J., Holzer, T. and Sime, D.G. (eds) (1988) *Proc. Sixth Int. Solar Wind Conf.*, High Altitude Observatory, NCAR, Boulder.

Parks, G.K. (1991) *Physics of Space Plasmas*. Addison-Wesley.

Priest, E. (ed)(1985) *Solar System Magnetic Fields*, Dordrecht: D. Reidel, pp. 224–56.

Russell, C.T. Hoppe, M.M. and Livesey, W.A. (1982). Overshoots in planetary bow shocks. *Nature*, **296**, 45–8.

Russell, C.T., Baker D.N. and Slavin, J.A. (1988). The magnetosphere of Mercury, in *Mercury* (eds F. Vilas, C.R. Chapman and M.S. Mathews) Tucson: University of Arizona Press.

Siscoe, G.L. (1979). Towards a comparative view of planetary magnetospheres, in *Solar System Plasma Physics*, Vol II (eds C.F. Kennel, L.J. Lanzerotti and E.N. Parker). Amsterdam: North Holland, 402 pp.

Slavin, J.A., Smith, E.J., Spreiter, J.R. and Starhara, S.S. (1985) solar wind flow about the outer planets: gas dynamic modeling of the Jupiter and Saturn bow shocks. *J. Geophys. Res.*, **90**, 6275–86.

Van Allen, J.A. (1990) Magnetospheres, cosmic rays and the interplanetary medium, in *The New Solar System* (eds J.K. Beatty and A. Chaikin). Sky Publishing.

Young, D.T. (1989). Space plasma mass spectroscopy below 60 KeV, in *Solar System Plasma Physics* (eds J.H. Waite, J.L. Burch and R.L. Moore). American Geophysical Union Publications, pp. 143–58.

Young, D.T., Marshall J.A., Burch, J.L. *et al.* (1989). A 360° field of view toroidal ion composition analyzer using time of flight, in *Solar System Plasma Physics* (eds J.H. Waite, J.L. Burch and R.L. Moore). American Geophysical Union Publications, pp. 171–80.

Cross references

Alfvén wave
Aurora
Comet: dynamics
Ion and neutral mass spectrometry
Ionosphere
Magnetospheres of the outer planets
Planetary torus
Plasma wave
Radiation belt
Solar corona
Solar wind
Thermal plasma instrumentation

PLASMA WAVE

A plasma is an electrically neutral mixture of electrons and ions in which the kinetic energy greatly exceeds the interaction energy between the particles. Plasmas are produced (1) by collisions whenever a gas is heated to over a few thousand degrees, and (2) by photoionization, for example by ultraviolet radiation from the Sun. Plasmas are destroyed by recombination. Because of the very low densities that exist in interplanetary space and the correspondingly low recombination rates, almost all of the material that exists between the Sun and the planets is a plasma. This includes the solar corona, which is the hot ionized outer atmosphere of the Sun; the solar wind, which is an ionized gas streaming outward from the Sun at supersonic speeds; planetary magnetospheres, which are hot energetic plasmas surrounding planets with strong magnetic fields; and planetary ionospheres, which are layers of ionized gas in the upper regions of planetary atmospheres.

As in any fluid, waves can propagate through a plasma. Because of the electrical character of the plasma medium, plasma waves are very complex. Some of these waves have electric and magnetic fields, and are similar to the electromagnetic waves in free space. These are called electromagnetic waves. Others are more like sound waves and have no magnetic field. These are called electrostatic waves, since the electric field can be derived from the gradient of an electrostatic potential ($\overline{E} = -\overline{\nabla}\,\phi$). Usually, electromagnetic waves have propagation speeds near the speed of light, whereas electrostatic waves have propagation speeds near the speed of sound.

In most space plasmas the collision frequencies are very low. This type of plasma, with essentially zero collision frequency and infinite

Table P10 The most common plasma wave modes

Plasma wave mode	Frequency range	Electromagnetic/ electrostatic	Polarization	Free energy source
Free-spaced (L,O) mode	$\omega > \omega_{pe}$	Electromagnetic	L	Beam, loss cone
Free-space (R,X) mode	$\omega > \omega_{R=0}$	Electromagnetic	R	Beam, loss cone
Electron plasma oscillations (Langmuir waves)	$\omega \simeq \omega_{pe}$	Electrostatic	–	Beam
Z mode	$\omega_{UHR} > \omega > \omega_{L=0}$	Electromagnetic, electrostatic near ω_{UHR}	R for $\omega > \omega_{pe}$ L for $\omega > \omega_{pe}$	Beam
Electron cyclotron waves	Bands near $\omega \simeq (n + \frac{1}{2})\omega_{ce}$	Electrostatic	–	Ring distribution (electrons)
Whistler mode	$\omega < \text{Min}\ \{\omega_{ce}, \omega_{pe}\}$	Electromagnetic, electrostatic near ω_{LHR}	R	Loss cone, beam above ω_{LHR}
Ion-acoustic mode	$\omega \lesssim \omega_{pi}$	Electrostatic	–	Drift between electrons and ions
Electrostatic ion cyclotron waves	Bands near $\omega \simeq (n + \frac{1}{2})\omega_{ci}$	Electrostatic	–	Ring distribution (ions) field-aligned currents
Electromagnetic ion cyclotron waves	$\omega << \omega_{ci}$	Electromagnetic	L	Pressure anisotropies

$\omega_{R=0} = \omega_{ce}/2 + ((\omega_{ce}/2)^2 + \omega_{pe})^{1/2}$
$\omega_{UHR} = (\omega_{ce}^2 + \omega_{pe}^2)^{1/2}$
$\omega_{L=0} = -\omega_{ce}/2 + ((\omega_{ce}/2)^2 + \omega_{pe}^2)^{1/2}$
$\omega_{LHR} \simeq (\omega_{ce}\ \omega_{ci})^{1/2}$ if $\omega_{pe} \gg \omega_{ce}$

mean free path, is called a collisionless plasma. The absence of collisions effectively eliminates the basic mechanism of energy and momentum exchange that normally exists between particles in a fluid. Under this circumstance, waves provide the primary mechanism for energy and momentum exchange. Waves then play a role somewhat similar to collisions in an ordinary gas. Whenever a sufficiently large deviation from thermal equilibrium occurs, waves grow spontaneously in the plasma. The non-equilibrium feature that gives rise to the wave growth is called a free energy source. Examples of free energy sources are beams and anisotropies in the velocity distribution of the particles. Once generated, the waves are eventually reabsorbed via a process known as collisionless damping. The wave growth and damping lead to an energy and momentum exchange. From very general principles it can be shown that the energy and momentum exchange acts to drive the plasma toward thermal equilibrium, very similar to collisions in an ordinary fluid. Waves therefore play a crucial role in maintaining the equilibrium state of the plasma.

Many different plasma wave modes exist in a plasma, particularly if the plasma has a magnetic field. These wave modes are usually associated with certain characteristic frequencies. The two primary characteristic frequencies of a plasma are the plasma frequency ω_p and the cyclotron frequency ω_c. A plasma frequency and a cyclotron frequency can be defined for each species present in the plasma. The electron plasma frequency is given by

$$\omega_{pe} = \left(\frac{e^2 n_e}{\epsilon_0 m_e} \right)^{1/2} \tag{P9}$$

where e is the electronic charge, n_e is the electron number density, ϵ_0 is the permittivity of free space and m_e is the electron mass. The electron plasma frequency is the characteristic oscillation frequency that occurs whenever electrons are perturbed from their equilibrium position in the plasma. The electron cyclotron frequency is given by

$$\omega_{ce} = \frac{eB}{m_e} \tag{P10}$$

where B is the magnetic field. The electron cyclotron frequency is the characteristic rotation frequency that occurs whenever an electron has a component of velocity perpendicular to the magnetic field. Comparable equations for the ion plasma frequency and ion cyclotron frequency are obtained by changing (e) to (i) in equations (P9) and (P10). In addition to the electron and ion plasma frequencies and cyclotron frequencies, it is convenient to define four additional characteristic frequencies. These are: the upper hybrid resonance frequency,

$$\omega_{UHR} = (\omega^2_{pe} + \omega^2_{ce})^{1/2} \tag{P11}$$

the lower hybrid resonance frequency,

$$\omega_{LHR} = (\omega_{ce}\ \omega_{ci})^{1/2} \tag{P12}$$

the right-hand cut-off,

$$\omega_{R=0} = \omega_{ce}/2 + ((\omega_{ce}/2)^2 + \omega^2_{pe})^{1/2} \tag{P13}$$

and the left-hand cut-off,

$$\omega_{L=0} = -\omega_{ce}/2 + ((\omega_{ce}/2)^2 + \omega^2_{pe})^{1/2} \tag{P14}$$

The relationships that these characteristic frequencies have to the various wave modes that exist in a plasma are summarized in Table P10. This table lists the commonly accepted name of the mode, the frequency range over which the mode can propagate, the electromagnetic/electrostatic character of the mode, the polarization (R,L) with respect to the magnetic field (when applicable) and the free energy source that can cause wave growth. It should be noted that Table P10 only applies to a plasma consisting of electrons and one positive ion species. If more than one positive ion species is present, then additional modes appear between adjacent pairs of ion cyclotron frequencies. For a further detailed discussion of the wave modes that can exist in a plasma, see Stix (1962) or Krall and Trivelpiece (1973).

Instrumentation

Space plasma wave measurements have been carried out by spacecraft-borne instrumentation for over 30 years. The first instruments specifically designed to study naturally occurring space plasma waves were launched on the Earth-orbiting Alouette 1 and Injun III satellites in 1962 (Barrington and Belrose, 1963; Gurnett and O'Brien, 1964). Since then many different types of plasma wave instruments have flown on Earth-orbiting and interplanetary spacecraft. These instruments usually have several characteristics in common. In order to distinguish between electromagnetic waves and electrostatic waves, both electric and magnetic fields must be measured. (The absence of a wave magnetic field indicates the wave is electrostatic.) Electric fields are usually detected by an electric dipole antenna that extends in opposite directions from the center of the spacecraft, as illustrated in Figure P28. The quantity measured is the voltage difference, $\Delta V = V_2 - V_1$, between the two antenna elements. The electric field component along the axis of the antenna is then given by $E = \Delta V / l_{eff}$, where l_{eff} is a quantity called the effective length. For wavelengths λ longer than the tip-to-tip length L of the antenna, the effective length is given by $l_{eff} = L/2$. A wide range of electric antenna lengths can be used, ranging from a fraction of a meter to over 200 m. Because the measured voltage ΔV increases with the antenna length, longer antennas are generally preferred since they give better sensitivity. A variety of mechanisms are used to extend the antenna. One technique uses centrifugal force to pull a fine wire

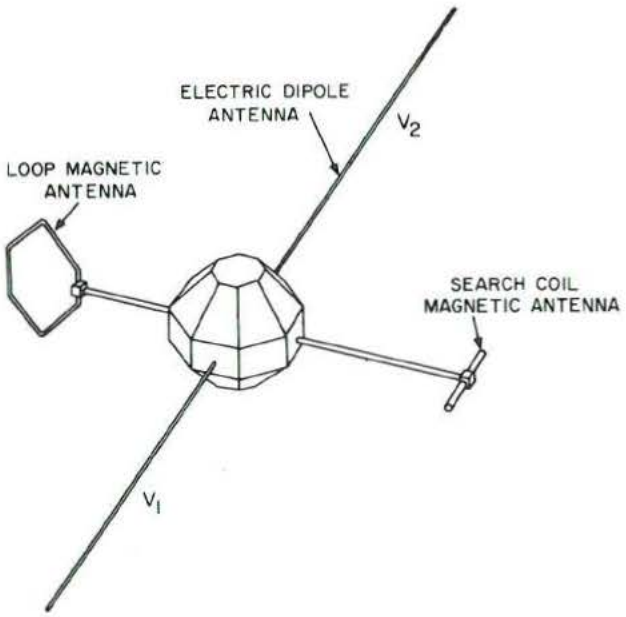

Figure P28 A typical antenna geometry for detecting space plasma waves. Electric fields are usually detected by an electric dipole antenna, and magnetic fields are detected by either a loop antenna or a search coil magnetometer.

radially outward from a fishing-reel type of dispenser in the spacecraft. This technique only works on spinning spacecraft. Another technique uses a motor-driven device to extrude a thin metal tape through a guide to form a rigid metal tube. This type of antenna works equally well on both spinning and non-spinning spacecraft. Sometimes small metal spheres with internal high impedance amplifiers are placed on the ends of the antenna to sense the potential in the plasma (Fahleson, 1967). In this case, the effective length is the center-to-center distance between the spheres.

Wave magnetic fields are usually detected using the magnetic induction principle, wherein a voltage is induced in a coil of wire by a time-varying magnetic field. The voltage induced is given by $V = N\mathrm{d}\Phi/\mathrm{d}t$, where $\Phi = AB$ is the magnetic flux through the coil, N is the number of turns, A is the cross-sectional area and B is the magnetic field strength. Two types of magnetic sensors are used. The first type is a loop antenna. Usually a loop antenna consists of a single turn, which minimizes the inductance and gives the maximum bandwidth. A transformer is usually used to couple the antenna to the electronics. The second type is a search coil magnetometer, which consists of a high-permeability rod surrounded by a sensing coil. The high-permeability rod acts to concentrate the magnetic flux through the coil, thereby increasing the sensitivity. Generally, loop antennas provide better sensitivities at higher frequencies, particularly above a few tens of kilohertz, whereas search coils provide better sensitivities at lower frequencies, below a few hundred hertz. To reduce interference from electrical systems on the spacecraft, magnetic field antennas must be mounted on booms away from the spacecraft body, as illustrated in Figure P28. In some cases multiple axis antennas are also used. Full three-axis measurements give information on the direction of propagation of a wave

The signals from the electric and magnetic antennas can be processed in a variety of ways. A typical block diagram of a plasma wave instrument is shown in Figure P29. Usually the antennas are connected to preamplifiers located close to the antennas. The preamplifiers are designed to provide low noise levels and to optimize the transmission of signals from the antennas to the main electronics package. The frequency range over which the antenna/preamplifier system must operate extends from the lowest characteristic frequencies of interest (usually f_{ci}) to the highest frequencies of interest (f_{pe} or f_{ce}). For planetary plasma wave investigations, this frequency range typically extends from a few hertz to a few megahertz.

Two different techniques are employed to process signals from electric and magnetic field sensors. In the first technique an onboard spectrum analyzer is used to generate spectrum amplitudes at a series of frequencies, $f_1, f_2, \ldots, f_n$. A spectrum analyzer of this type is shown in the top portion of the block diagram in Figure P29. The purpose of the onboard spectrum analysis is to provide continuous low-resolution survey spectrums using relatively modest telemetry rates, typically a few hundred bits per second. In the second technique a wideband receiver is used to transmit electric or magnetic field waveforms directly to the ground. The onboard signal processing is minimal, and the spectrum processing (Fourier analysis) is performed by ground-based computers. A wideband receiver is shown at the bottom of the block diagram in Figure P29. The main purpose of the wideband receiver is to limit the bandwidth of the signal and to control the amplitude of the signal by means of an automatic gain control. The waveform transmission can be either analog or digital. The advantage of the waveform measurements is the very high resolution. Since the entire waveform is transmitted, the resolution in frequency and time is limited only by the uncertainty principle ($\Delta\omega\Delta t \approx 1$). The disadvantage is that the telemetry rates are extremely high, often several hundred kbits per second or more. For this reason, wideband waveform transmissions are often of limited duration (60 s or less), thereby restricting the waveform measurements to a few specific samples, rather than continuous coverage. In this respect the onboard spectrum analysis and the wideband technique are complementary. The spectrum analyzer provides continuous low-resolution survey measurements, and the wideband receiver provides high-resolution spectrums for selected time intervals.

Observations

Spacecraft plasma wave observations have now been obtained at seven planets (Venus, Earth, Mars, Jupiter, Saturn, Uranus and Neptune). The most extensive measurements have been performed in the vicinity of Earth. Since the first such measurements in 1962 many spacecraft have provided plasma wave measurements in Earth orbit. These spacecraft have explored most of the near-Earth environment, with trajectories ranging from low-altitude orbits near the Earth, to highly eccentric orbits extending well beyond the orbit of the Moon. Plasma wave observations at the other planets are much more limited, and it is these measurements that will be emphasized here, since they are at the frontier of present day research. Of the various spacecraft that have flown to the other planets, the Voyager 1 and 2 mission to the giant planets, Jupiter, Saturn, Uranus and Neptune, has probably contributed the most to our expanding knowledge of space plasma waves. The giant planets, like the Earth, have strong magnetic fields and intense radiation belts, which make them a rich source of plasma waves. For the initial Voyager reports of plasma wave observations at the giant planets, see Scarf, Gurnett and Kurth (1979), Scarf *et al.* (1982), Gurnett, Kurth and Scarf (1979a, 1981) and Gurnett *et al.* (1986, 1989). The only other spacecraft that has provided plasma wave measurements at the giant planets is Ulysses, which flew by Jupiter in 1992. For the initial report of the Ulysses plasma wave observations, see Stone *et al.* (1992). The remaining two planets, Venus and Mars, have negligible internal magnetic fields and therefore fewer types of plasma wave phenomena. The first measurements of plasma waves in the vicinity of Venus were provided by the Pioneer Venus spacecraft, which was placed in orbit around Venus on 4 December 1979. The first report on the Pioneer Venus plasma wave observations was given by Scarf, Taylor and Green (1979). The only other spacecraft that has provided plasma wave observations in the vicinity of Venus is Galileo, which flew by Venus on 10 February 1990. For a report on the Galileo Venus plasma wave observations, see Gurnett *et al.* (1991). At Mars the first, and only, plasma wave measurements were obtained by the Phobos 2 spacecraft, which was placed in orbit around Mars on 29 January 1989. An initial report on the Phobos 2 plasma wave observations is given by Grard *et al.* (1991).

Since there are so many planets to review, no attempt will be made to describe the observations in detail at each planet. Instead, the observations will be organized according to the various types of plasma waves observed, ordered according to decreasing distance from the planet, starting from the Sunward side of the planet, and ending in the region near the closest approach. No discussion is given of electromagnetic radiation that can escape to great distances from the planet, since these waves are usually regarded as radio astronomi-

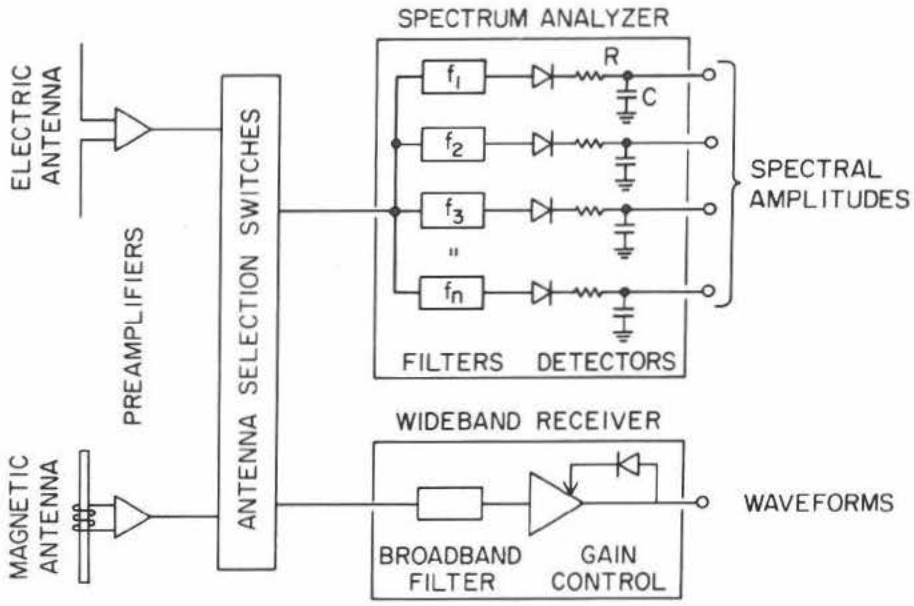

Figure P29 A block diagram of a typical plasma wave instrument. These instruments often consist of an onboard spectrum analyzer which gives low-resolution continuous spectrums, and a wideband waveform receiver which gives very high-resolution spectrums for selected intervals.

cal emissions. For a review of planetary radio emissions see Gurnett (1992).

Electron plasma oscillations and ion acoustic waves

The solar wind flows outward from the Sun at a nearly constant speed of about 400 km s^{-1}. At this speed the solar wind flow is supersonic. When the solar wind encounters a large object such as a planet, a shock wave is formed, very similar to the shock wave that forms upstream of an airplane in supersonic flight. This shock is called the bow shock. The approximate shape of the shock is shown in Figure P30. If the planet has no internal magnetic field, as in the case of Venus and Mars, the planet and its surrounding atmosphere and ionosphere act as the obstacle. The radial distance to the nose of the shock is then only slightly larger than the radius of the planet. If the planet has a strong internal magnetic field, as in the case of the Earth and the giant planets, the magnetic field acts as the obstacle. The position of the shock is then controlled by the strength of the planetary magnetic field. The interface between the solar wind and the planetary magnetic field is called the magnetopause (Figure P30). At Jupiter, for example, the nose of the shock is typically at 80 to 120 R_J (where R_J is the radius of the planet), and the magnetopause is at 50 to 70 R_J.

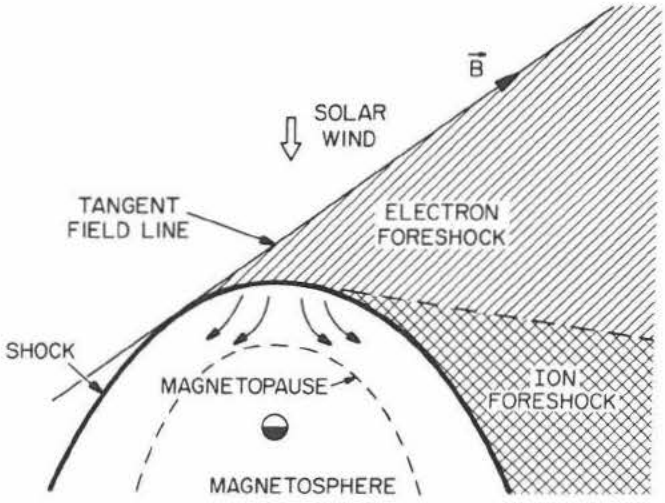

Figure P30 A sketch of the various boundaries and regions that occur in the solar wind upstream of a planet. Since the solar wind is supersonic, a shock wave forms upstream of the planet. Electrons and ions energized at the shock escape upstream into regions known as the electron foreshock and the ion foreshock.

At the shock the plasma is strongly heated and some of the electrons and ions escape upstream into the solar wind. Because the escaping particles are guided along the magnetic field lines by magnetic forces, these particles are confined to a region upstream of the shock called the foreshock. Usually the escaping electrons have very high speeds, typically 10^4 to 10^5 km s^{-1}, which is much greater than the solar wind speed. At these very high velocities, the region accessible to the backstreaming electrons is essentially delineated by the magnetic field lines tangent to the shock (Figure P30). This region is called the electron foreshock. The escaping ions, because of their higher mass, have much lower velocities, more nearly comparable to the solar wind speed. The region accessible to the backstreaming ions is therefore angled backward substantially from the tangent field line (Figure P30). This region is called the ion foreshock.

Because the backstreaming electrons constitute a beam, these particles can excite electron plasma oscillations, also sometimes called Langmuir waves (Table P9). Electron plasma oscillations excited by electrons streaming into the solar wind were first discovered by Scarf *et al.* (1971) upstream of the Earth's bow shock. Since then similar electron plasma oscillations have been discovered at Venus and Mars and at all four of the giant planets. A multichannel plot illustrating the occurrence of electron plasma oscillations upstream of Jupiter's bow shock is shown in Figure P31. These data are from the low-rate spectrum analyzer onboard Voyager 1. The enhanced emissions in the 5.62-kHz channel from about 12 : 18 to 12 : 27 UT are electron plasma oscillations. The electron plasma frequency f_{pe} during this interval was about 5.5 to 6.0 kHz. The onset of the plasma oscillations at 12 : 18 UT corresponds to the crossing of the tangent field line, and the termination at 12 : 27 UT corresponds to the crossing of the bow shock.

The frequency of upstream electron plasma oscillations generally decreases with increasing distance from the Sun. As can be seen from equation (P9), the electron plasma frequency is proportional to the square root of the electron density. Since the solar wind density varies roughly as $1/R^2$, where R is the distance from the Sun, the

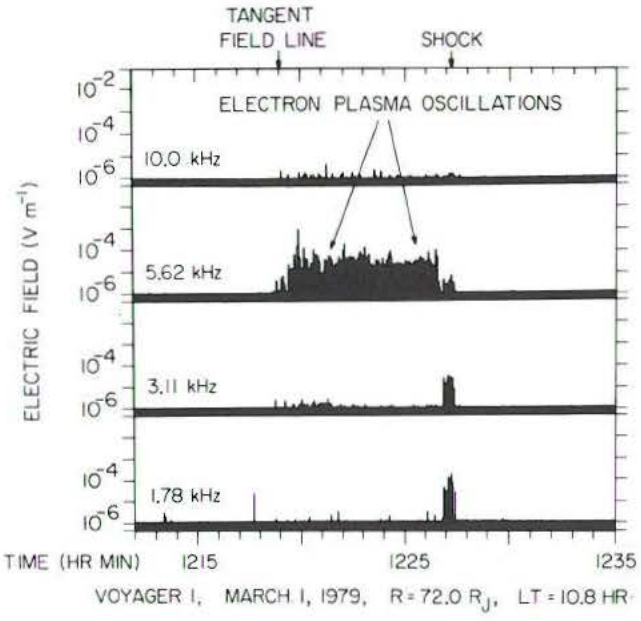

Figure P31 An example of electron plasma oscillations in the solar wind upstream of Jupiter. These waves occur in the electron foreshock and are produced by energetic (~ 1 to 10 keV) electron beams escaping into the solar wind from the bow shock.

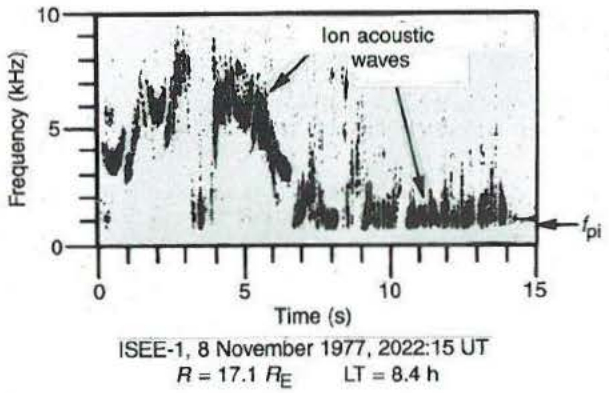

Figure P32 A high-resolution frequency–time spectrogram of ion acoustic waves observed in the solar wind upstream of the Earth's magnetosphere. These waves are produced by energetic (~ 10 keV) ions escaping into the solar wind from the bow shock.

electron plasma frequency varies roughly as $1/R$. At Venus the electron plasma frequency is typically about 30 kHz, whereas at Neptune the electron plasma frequency is about 700 Hz. The electric field strength of the plasma oscillations also decreases with increasing distance from the Sun. At Venus and Earth the peak field strengths are about 1 mV m^{-1}, whereas at Neptune the peak field strengths are about 30 to 100 μV m^{-1}.

In addition to electron plasma oscillations, another type of wave also occurs upstream of planetary bow shocks. These waves were first detected upstream of the Earth's bow shock by Scarf *et al.* (1970) and are called ion acoustic waves (Gurnett and Frank, 1978). Ion acoustic waves are very similar to sound waves in an ordinary gas and are driven by ions escaping from the shock. Since these waves are driven by ions, they are confined to the ion foreshock. A wideband spectrogram of ion acoustic waves detected by the Voyager 1 spacecraft upstream of Jupiter's bow shock is shown in Figure P32. As can be seen, the ion acoustic waves have relatively narrow bandwidths and switch on and off abruptly. The abrupt onsets and terminations indicate that the mode is very close to marginal instability. The peak frequencies of the ion acoustic waves (~ 2 kHz) are well below the electron plasma frequency ($f_{pe} \sim 5$ kHz) but still above the ion plasma frequency ($f_{pi} \sim 120$ Hz). As can be seen from Table P9, the ion acoustic mode can only propagate at frequencies below the ion plasma frequency. This discrepancy is believed to occur because the waves have very short wavelengths, thereby introducing Doppler shifts due to the motion of the solar wind. For a wave of wavelength λ and frequency f in the plasma rest frame, the frequency f' detected in the spacecraft rest frame is given by

$$f' = f + \frac{V_{sw}}{\lambda} \cos \theta_{kv} \qquad \text{(P15)}$$

where V_{sw} is the solar wind speed and θ_{kv} is the angle between the propagation vector $\vec{k}$ and the solar wind velocity. The shortest wavelength that can exist in a plasma is $\lambda_{min} = 2\pi\lambda_D$, where λ_D is a characteristic length called the Debye length. For the plasma parameters that exist in the solar wind upstream of Jupiter, the shortest wavelength is about $\lambda_{min} \approx 240$ m. The maximum Doppler shift, which is given by the second term on the right-hand side of equation (P11), is then about 1.7 kHz, which is comparable to the highest frequencies observed. Ion acoustic waves have only been reported upstream of the bow shocks at Earth, Mars and Jupiter. For unknown reasons, possibly due to instrumental limitation, ion acoustic waves have not been observed upstream of the bow shocks at Venus, Saturn, Uranus or Neptune.

The bow shock crossings at Venus, Earth, Mars, and all four of the giant planets can be easily identified in the plasma wave data by an intense broadband burst of electric field noise at the shock. This noise was first discovered in the Earth's bow shock by Fredricks *et al.* (1968). A wideband frequency–time spectrogram showing the shock-related electric field noise observed during the Voyager 1 crossing of Jupiter's bow shock is given in Figure P33. This is the same shock crossing shown in Figure P31. Note the electron plasma oscillations at ~ 6 kHz, increasing slowly in frequency as the spacecraft approaches the shock. The electric field noise at the shock extends up to a frequency of about 3 kHz and has a peak broadband intensity of about 1 mV m^{-1}. This noise is believed to be caused by solar wind ions that are magnetically reflected by the shock, thereby forming a gyrating ion beam that excites electrostatic waves via a two-stream instability. Currents flowing along the shock surface may also in some cases contribute to the generation of electrostatic waves. Earlier it was thought that these electrostatic waves played the dominant role in heating the plasma at collisionless shocks (Fredricks *et al.*, 1968). However, more recent studies by Scudder *et al.* (1986) and others suggest that these waves probably act only to thermalize the particle distribution, and that other processes, such as acceleration by quasi-static electric fields and magnetic reflection, are primarily responsible for converting the directed solar wind flow into a heated distribution at the shock.

Trapped continuum radiation

After the shock, the next boundary of interest is the magnetopause. This boundary forms the effective obstacle for the solar wind flow around the planet and is shown by a dashed line in Figure P30. Because the planetary magnetic field provides most of the pressure inside of the magnetosphere, an abrupt drop in the plasma density occurs at the magnetopause, thereby forming a low-density magnetospheric cavity. Since the electron plasma frequency is lower in the magnetosphere than in the solar wind, electromagnetic radiation can be trapped in the magnetospheric cavity. This trapped radiation was first discovered in the Earth's magnetosphere by Gurnett and Shaw (1973) and is called continuum radiation. Since then, trapped continuum radiation has been observed at three of the giant planets, Jupiter, Saturn and Uranus. No trapped continuum radiation was observed at Neptune, probably because the Voyager plasma wave instrument did not have sufficient sensitivity to detect this radiation at Neptune. The trapped continuum radiation at Jupiter is one of the most intense emissions observed at any of the planets. Since no magnetospheric cavity exists at Venus and Mars, trapped continuum radiation cannot occur at either of these planets. For a review of continuum radiation in planetary magnetospheres see Kurth (1991).

An example of trapped continuum radiation is shown in Figure P34. This spectrogram shows the Voyager 1 crossing of the magneto-

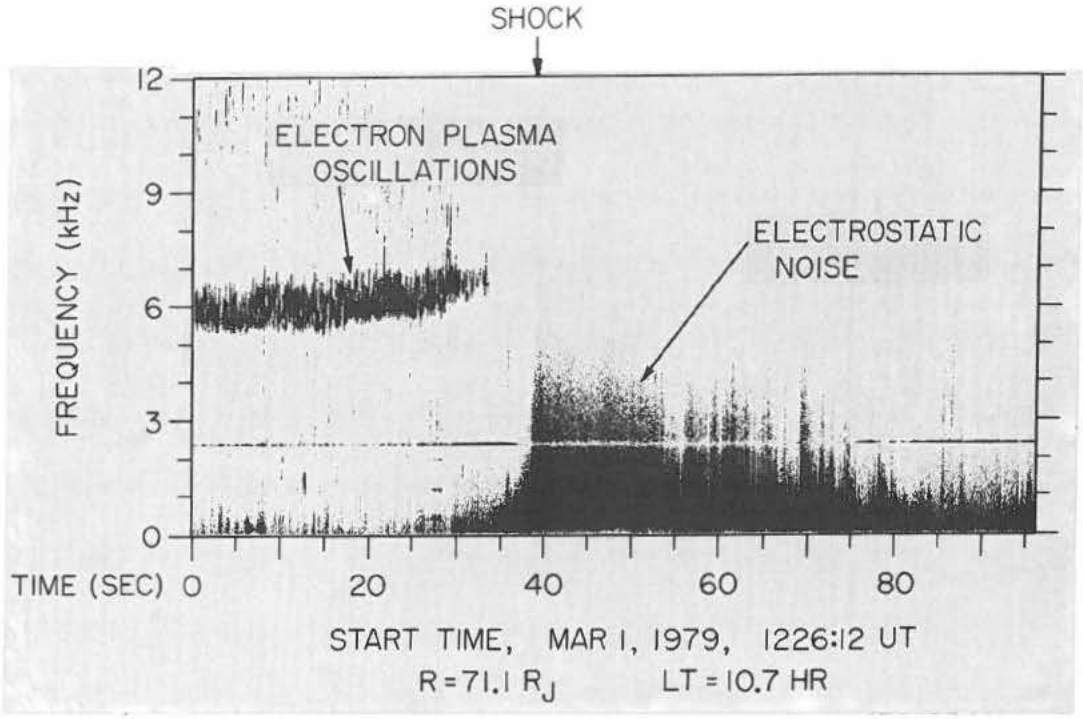

Figure P33 The Voyager 1 inbound crossing of Jupiter's bow shock. An abrupt burst of broadband electric field noise can be seen at the shock. This noise is believed to be caused by ion beams gyrating back into the solar wind from the shock. Electron plasma oscillations can also be seen upstream of the shock.

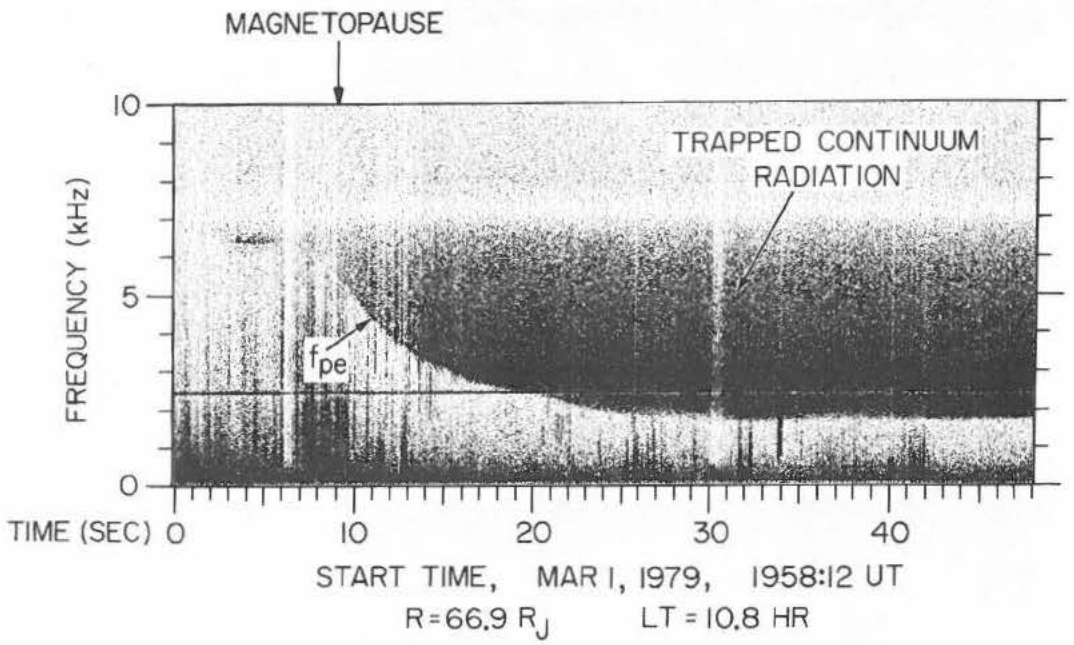

Figure P34 The inbound Voyager 1 crossing of Jupiter's magnetopause. The intense band of noise from about 2 to 7 kHz is continuum radiation trapped in the low-density magnetospheric cavity. The low-frequency cut-off of the continuum radiation is at the electron plasma frequency, f_{pe}.

pause at Jupiter. The continuum radiation consists of the dark band of noise extending upward from about 1 kHz, gradually fading into the receiver background noise above about 7 kHz. The sharp, low-frequency cut-off of the radiation at f_{pe} is believed to be caused by the reflection of free space (L,O) mode electromagnetic waves at the local electron plasma frequency. As can be seen from Table P10, the free space L,O mode can only propagate at frequencies $f > f_{pe}$. Free space (R,X) mode radiation is also most likely present. However, the low-frequency cut-off of the R–X mode is always above f_{pe}, so the L–O mode determines the low-frequency cut-off. The monotonic decrease in the low-frequency cut-off, from about 6.2 to 1.8 kHz over a period of about 20 s, is caused by the rapidly declining plasma

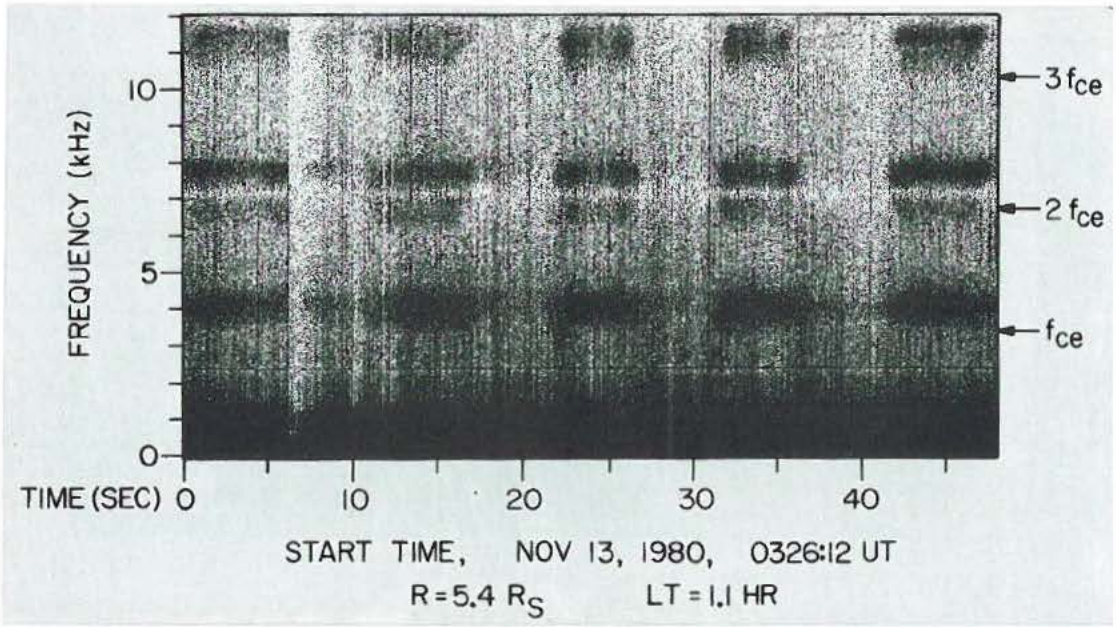

Figure P35 An example of electrostatic electron cyclotron harmonic (ECH) waves in Saturn's magnetosphere. These emissions occur in narrow bands slightly above harmonics of the electron cyclotron frequency, f_{ce}.

density as the spacecraft passes through the magnetopause. Note from equation (P9) that the electron plasma frequency is proportional to the square root of the electron density. The thickness of the magnetopause is controlled mainly by the cyclotron radius of magnetosheath ions as they gyrate into the region of strong field inside the magnetosphere. Continuum radiation comparable to Figure P33 is observed throughout the magnetospheric cavity of Jupiter. Once generated, the radiation is believed to undergo repeated reflections from the walls of the cavity, eventually building up to an equilibrium level throughout the cavity. Small random Doppler shifts caused by repeated reflections from the walls of the magnetospheric cavity, which are continuously in motion, are believed to spread the radiation into a nearly continuous spectrum, hence the term continuum.

Electron cyclotron and upper hybrid waves

For the magnetized planets, the magnetic field within the magnetosphere is generally much stronger than in the solar wind. The electron cyclotron frequency then plays an important role in controlling the types of waves that are generated. In the Earth's magnetosphere it has been known for many years that strong electrostatic emissions are generated near harmonics of the electron cyclotron frequency (Kennel *et al.*, 1970; Shaw and Gurnett, 1975). These emissions are part of a band structure that is often referred to as electron cyclotron waves (Table P10). The free energy source of these waves consists of electrons with a loss cone or ring type of distribution function. Loss-cone velocity distributions are a characteristic feature of planetary radiation belts. Charged particles moving within a well-defined cone of angles around the magnetic field (the loss cone) strike the atmosphere and are lost from the system, thereby producing a hole in the particle velocity distribution.

Electron cyclotron waves are found in the magnetosphere of the Earth and all the giant planets. Typically these waves are most intense near half-integral harmonics $(n + \frac{1}{2})f_{ce}$ of the electron cyclotron frequency. Usually the $(n + \frac{1}{2})f_{ce}$ waves occur in two distinct frequency ranges, the first near low-order half-integral harmonics of the electron cyclotron frequency (i.e. $\frac{3}{2}f_{ce}$, $\frac{5}{2}f_{ce}$, etc.), and the second near the upper hybrid resonance frequency, when $(n + \frac{1}{2})f_e \simeq f_{UHR}$. The low-order harmonics are often called electron cyclotron harmonic (ECH) waves, and the emissions near the upper hybrid frequency are called upper hybrid resonance (UHR) waves. The emission frequencies depend in a complicated way on the densities and temperatures of the cold and hot components of the plasma, and are almost never exactly at $(n + \frac{1}{2})f_{ce}$. The half-integral notation, $\frac{3}{2}$, $\frac{5}{2}$, etc., is mainly just a convenient label to identify the emission band.

A spectrogram illustrating examples of low-order ($\frac{3}{2}$,$\frac{5}{2}$ and $\frac{7}{2}$) ECH emissions in the magnetosphere of Saturn is shown in Figure P35. The emission frequencies in this case are slightly above the electron cyclotron harmonics. Considerable fine structure can be seen within the emission bands. Electron cyclotron harmonic emissions of this type are typical of all the ECH observations at the giant planets. Usually, the emissions are strongest in a narrow band slightly above the electron cyclotron harmonics. A spectrogram illustrating an example of UHR emissions in the outer region of Jupiter's magnetosphere is shown in Figure P36. The UHR emissions in this case consist of very sharply defined bands near the lower edge of the trapped continuum radiation. The bands switch on and off as plasma density variations cause the upper hybrid resonance frequency to sweep past half-integral harmonics of the electron cyclotron frequency. Strong emissions occur whenever the condition $(n + \frac{1}{2})f_{ce} \simeq f_{UHR}$ is satisfied. The frequency spacing between the bands is roughly the electron cyclotron frequency.

A striking characteristic of both the ECH and UHR waves is their close confinement to the magnetic equator. Figure P37a shows a multichannel plot of electric field intensities from the Voyager 1 pass through the inner region of the Jovian magnetosphere. The ECH and UHR emissions are identified by circles. Figure P37b shows the magnetic latitude λ_m. The magnetic latitude oscillates up and down due to the rotation of Jupiter's magnetic dipole field, which is tilted at an angle of about 10° with respect to the rotational axis. As can be seen, the ECH and UHR waves occur in sharply localized regions centered almost exactly on the magnetic equator crossings. This narrow confinement to a region only 1 or 2 degrees from the magnetic equator is a characteristic feature of all the ECH and UHR observations at the giant planets. A similar effect also occurs in the Earth's magnetosphere, although not as dramatically as at the giant planets.

The reason that the ECH and UHR waves are confined to a narrow region near the magnetic equator is still a subject of investigation. Based on terrestrial studies it is believed that two factors are responsible. First, it is known that the electrons responsible for generating the waves have pitch angles near 90°. Due to the laws governing the motion of trapped radiation belt particles (conservation of the first and second adiabatic invariants), particles with pitch angles near 90° are closely confined to the vicinity of the magnetic equatorial plane. Since this type of highly anisotropic velocity distribution (with pitch angles near 90°) is required to generate the ECH and UHR waves, large wave growth can only occur near the magnetic equator. Second, ray tracing studies show

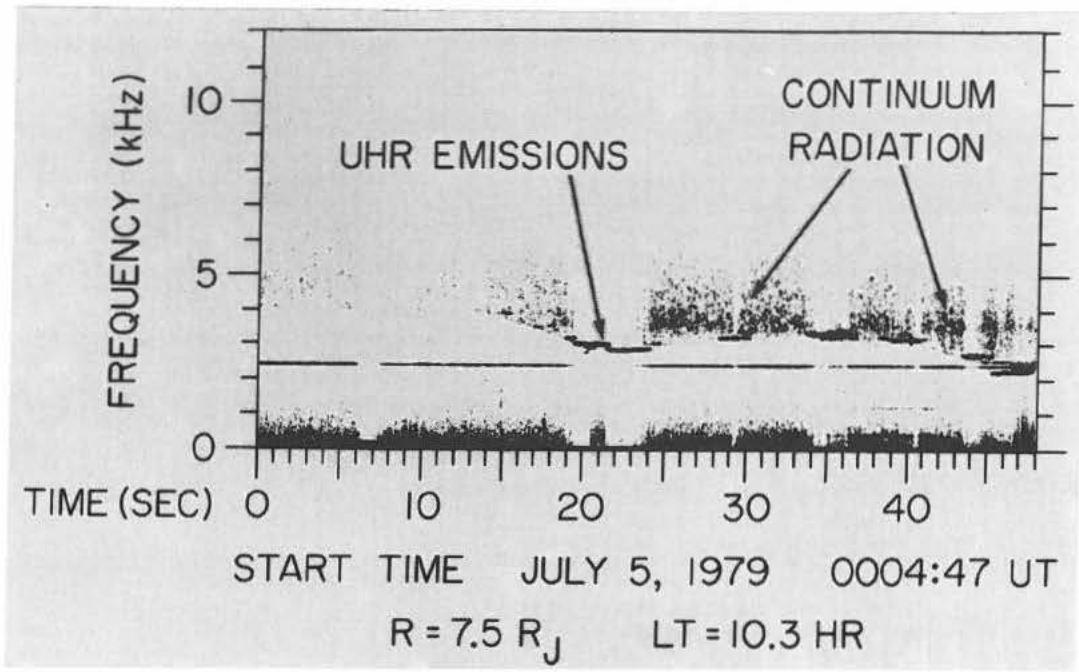

Figure P36 An example of upper hybrid resonance (UHR) emissions in Jupiter's magnetosphere. These emissions occur in narrow bands near the upper hybrid resonance frequency, f_{UHR}.

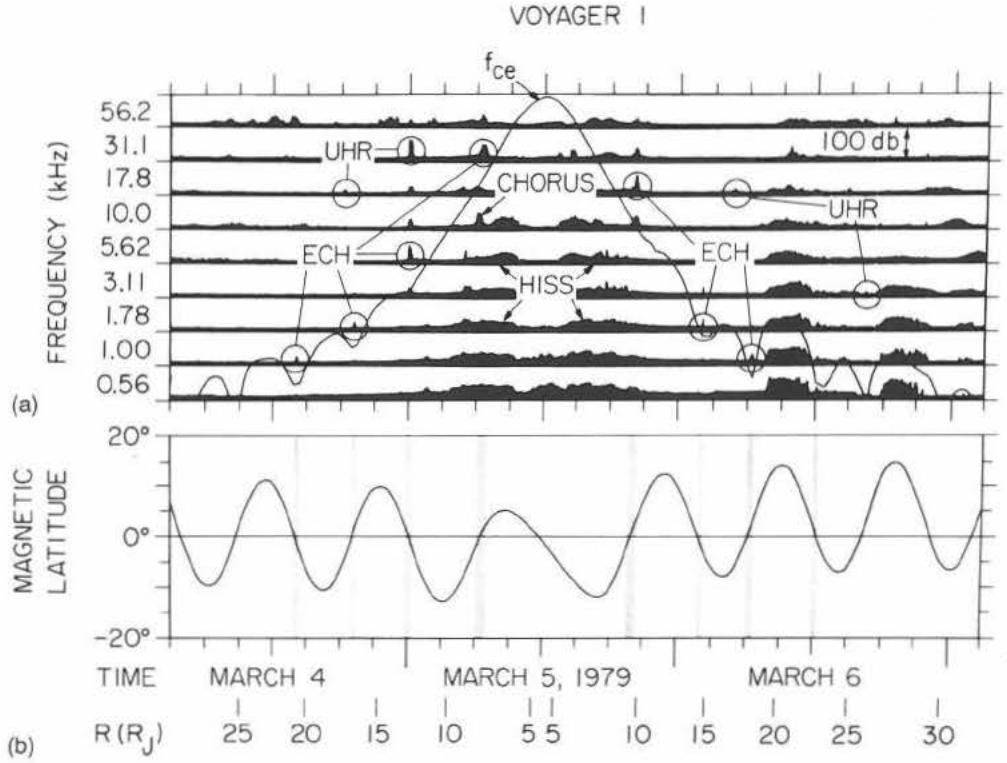

Figure P37 (a) Electric field intensities observed during the Voyager 1 pass through the inner region of the Jovian magnetosphere and (b) the magnetic latitude. Both ECH and UHR waves always occur very close to the magnetic equator.

that the electron cyclotron waves tend to be guided along the magnetic equator. This guiding effect is believed to confine the wave growth to a narrow region along the magnetic equatorial plane.

One may ask what role these electrostatic waves play in the magnetospheres of the giant planets. In the terrestrial magnetosphere, for many years it has been thought that electron cyclotron waves control the loss of trapped radiation belt electrons by scattering particles into the loss cone (Kennel *et al.*, 1970). It seems likely that similar processes are operative at the giant planets. Unfortunately, adequate measurements are not available from the Voyager plasma data in the proper electron energy range (a few hundred eV to several tens of keV) to evaluate this loss mechanism. In the Earth's magnetosphere, UHR emissions are also believed to be a source of free-space electromagnetic radiation. The generation mechanism is believed to involve a mode conversion process by which UHR waves are converted to escaping electromagnetic (L, O mode) radiation. The mode conversion process can be either linear (Jones, 1980) or nonlinear (Melrose, 1981). Trapped continuum radiation is thought to be produced by this mode conversion process (Kurth, 1991).

Whistler-mode emissions

Whistlers are one of the oldest and best-known terrestrial plasma wave phenomena. Whistlers were first observed by ground-based radio receivers (Barkhausen, 1919). The modern theory of whistlers was first proposed by Storey (1953). According to Storey's theory, low-frequency electromagnetic radiation from a lightning discharge is guided along the magnetic field lines through the magnetospheric plasma. Because of the peculiar nature of electromagnetic wave propagation at frequencies below the electron cyclotron frequency, the higher frequencies propagate faster than the lower frequencies. Thus, the broadband impulsive signal produced by a lightning flash is converted into a whistling tone, hence the term 'whistler'. The plasma wave mode involved in the propagation of whistlers is called the whistler mode. Whistler-mode waves are right-hand polarized and propagate at frequencies below either f_{ce} or f_{pe}, whichever is smaller (see Table P10). The whistler mode is highly anisotropic and has a number of unusual characteristics, one of which is that the index of refraction goes to infinity along a cone of directions called the resonance cone (Stix, 1962). This highly anisotropic characteristic accounts for the fact that the wave energy is guided approximately along the magnetic field (see Whistler).

In addition to lightning-generated whistlers, whistler-mode waves can also be spontaneously generated in a magnetized plasmas. These waves are called whistler-mode emissions. Whistler-mode emissions are a common feature of the terrestrial magnetosphere and occur in the magnetospheres of all the giant planets. These emissions are mainly generated in the inner regions of the magnetosphere where the loss cone in the trapped energetic electron distribution provides an effective free energy source. From very general principles (Brice, 1964), it can be shown that the growth of whistler-mode waves leads to a decrease in the pitch angle of resonant electrons, thereby driving the particles toward the loss cone. The growth of whistler-mode waves is widely believed to be the dominant mechanism responsible for the loss of energetic electrons from planetary radiation belts. In a classic paper Kennel and Petschek (1966) showed that the growth of whistler-mode waves puts an upper limit on the energetic electron intensities that can exist in planetary radiation belts.

A representative spectrum of whistler-mode emissions in the inner region of Jupiter's magnetosphere is shown in Figure P38a. This spectrum was obtained in the Io plasma torus, which is a dense torus of plasma produced by gases escaping from Jupiter's moon Io (see Planetary Torus). The plasma in the Io torus is extremely energetic and produces very intense whistler-mode emissions, among the most intense ever observed in a planetary magnetosphere. Two types of emissions are observed, called 'hiss' and 'chorus'. The hiss is an essentially structureless emission. When the hiss signals are played through an audio speaker, they make a steady hissing sound, hence the term 'hiss.' According to current ideas, whistler-mode hiss is believed to represent a fully developed turbulent spectrum in which the wave growth and loss has achieved a steady state equilibrium. In contrast to the whistler-mode hiss, chorus emissions are highly structured. A wideband frequency–time spectrogram of chorus is shown in Figure P39. The term 'chorus' is an old term (Allcock, 1957), and has its origins in the term 'dawn chorus' which refers to the sounds made by a roosting flock of birds at daybreak. The reasons for the complex spectral structure, usually consisting of many discrete

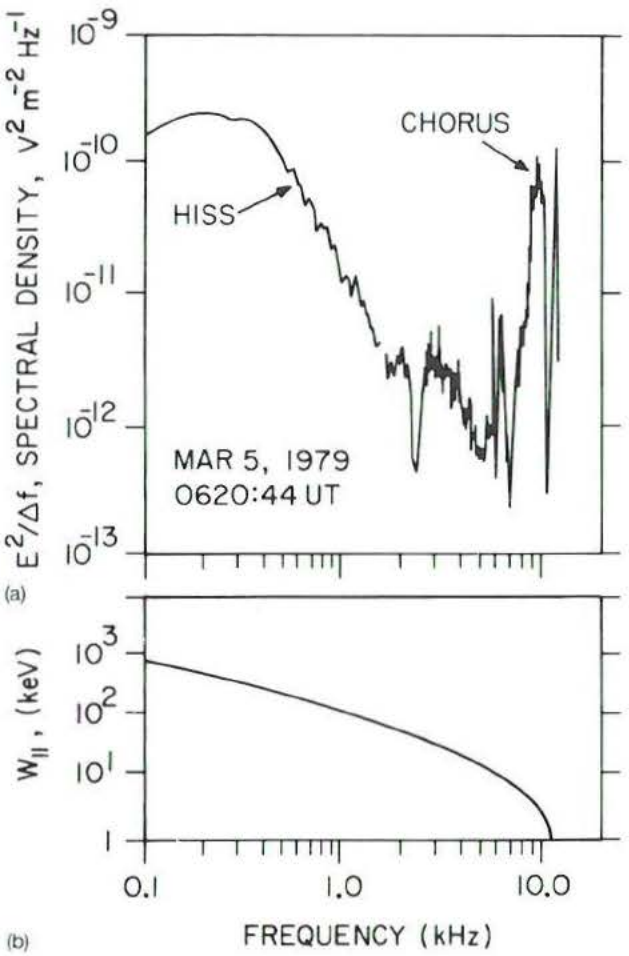

Figure P38 (a) An electric field spectrum of whistler-mode hiss and chorus emissions in Jupiter's Io torus. (b) The energy $W_{\|}$ of electrons that are in cyclotron resonance with these waves. The hiss tends to interact with very energetic electrons (~ 100 to 1000 keV), whereas the chorus interacts with much lower energies (~ 1 to 10 keV).

narrowband tones rising in frequency, is poorly understood. The current view is that the waves grow to such large amplitudes that local nonlinear processes play a dominant role in controlling the evolution of the wave. Computer simulations show that particles trapped in the wave field produce isolated wave packets, each of which evolves somewhat differently in time and space.

It is instructive to comment on the electron energies involved in the generation of hiss and chorus. Whistler-mode wave growth proceeds via a resonant process in which a constant force is experienced by a particle undergoing cyclotron motion along a magnetic field line, thereby leading to a deceleration (or acceleration) of the particle and a growth (or damping) of the wave. This process is called cyclotron resonance. The general condition for cyclotron resonance is

$$v_{\|\mathrm{Res}} = \frac{\omega - n\,\omega_{ce}}{k_{\|}} \qquad \text{(P16)}$$

where $v_{\|\mathrm{Res}}$ is the parallel resonance velocity (the symbol $\|$ refers to the component parallel to the magnetic field), ω is the wave frequency, $k_{\|}$ is the parallel component of the wave vector and n is an integer. For whistler-mode waves, the $n = 1$ term is usually most important. This resonance is called the first-order cyclotron resonance and occurs when both the wave and the particles (electrons) are rotating in the right-hand sense with respect to the magnetic field. From the propagation characteristics of the wave, $\omega(k)$, one can calculate the parallel energy $W_{\|}$ of the resonant electrons. The parallel resonance energy for whistler-mode emissions at Jupiter is

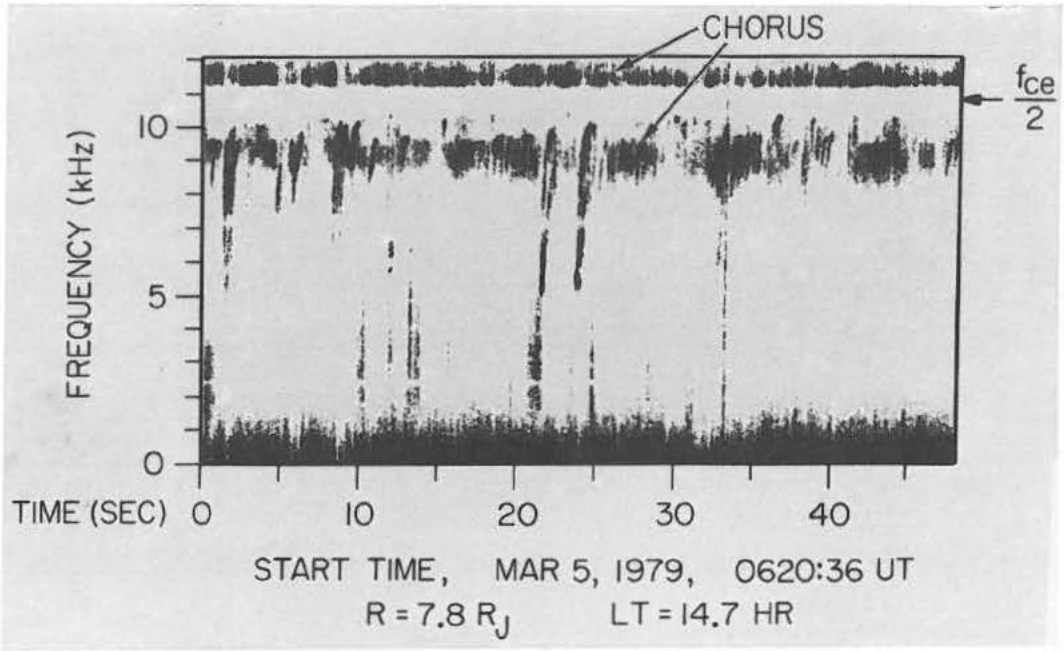

Figure P39 A high-resolution frequency–time spectrogram of chorus emissions. These emissions are highly structured and often consist of narrowband tones rising in frequency with increasing time. Chorus often has a sharp notch in the spectrum at one-half of the electron cyclotron frequency, $f_{ce}/2$.

shown in Figure P38b. As can be seen, the resonance energy decreases rapidly with increasing frequency. The energy of the electrons interacting with the hiss tends to be very high, 100 to 1000 keV, whereas the energy of the electrons interacting with the chorus tends to be much lower, 1–10 keV. This trend, for hiss to resonate with high energies and chorus to resonate with low energies, is typical of whistler-mode emissions at all of the giant planets.

In addition to Earth, three of the giant planets, Jupiter, Saturn and Uranus, have intense whistler-mode hiss and chorus emissions. These emissions occur in the inner regions of the magnetosphere where the trapped radiation belt electron intensities are the highest. The existence of whistler-mode emissions at Neptune is unclear. Some very weak emissions were observed in the spectrum analyzer data that are probably whistler-mode hiss. However, no chorus was observed in any of the wideband data. The absence of chorus at Neptune could be due to the low radiation belt intensities, which were the lowest of any of the giant planets. It can be shown that the growth rate of whistler-mode emissions increases in direct proportion to the intensity of the resonant electron. The extremely low whistler-mode emission intensities at Neptune could therefore be due to the low radiation belt electron intensities. On the other hand, the spacecraft did not pass through the equatorial region of the radiation belt where the highest wave amplitudes would be expected. Thus, it may be that strong whistler-mode emissions were present in the magnetosphere of Neptune, but the spacecraft did not pass through the proper region to observe these waves.

A third type of whistler-mode emission also occurs in planetary magnetospheres. This emission occurs in the auroral regions and is called auroral hiss. Auroral hiss is a nearly structureless emission and is believed to propagate at wave normal angles near the resonance cone. Near the resonance cone the whistler mode is very nearly electrostatic, with small magnetic fields, short wavelengths and low propagation speeds. These short-wavelength, quasi-electrostatic, whistler-mode waves are sometimes called lower hybrid waves, since they become completely electrostatic at the lower-hybrid resonance frequency, f_{LHR}. Because of the low propagation velocity, auroral hiss can be excited by beams, very similar to electron plasma oscillations. Auroral hiss has been extensively studied in the Earth's magnetosphere, where it has been shown that the emissions are produced by the same electron beams that produce the auroral light emission, hence the term 'auroral hiss.' Auroral hiss has also been observed at Jupiter by Voyager 1 (Gurnett *et al.*, 1979) and by Ulysses (Stone *et al.*, 1992). In both cases the identification was based on the similarity to terrestrial auroral hiss and not on a direct correlation with the aurora on Jupiter. No auroral hiss was observed at Saturn, Uranus or Neptune, most likely because the spacecraft did not pass through the proper region to observe such emissions.

Electrostatic ion cyclotron waves

Electrostatic ion cyclotron waves occur in discrete bands between harmonics of the ion cyclotron frequency (Table P10), very similar to electron cyclotron waves, which occur between harmonics of the electron cyclotron frequency. One of the unique features of the electrostatic ion cyclotron mode is that it is driven unstable by relatively weak field line currents. This feature led Kindel and Kennel (1971) to predict that electrostatic ion cyclotron waves would be produced by field-aligned currents over the Earth's auroral regions. The existence of such waves was subsequently confirmed by Kintner, Kelley and Mozer, (1978), using data from the polar orbiting S3–3 satellite. A representative spectrum of electrostatic ion cyclotron waves observed along the Earth's auroral field lines is show in Figure P40. Strong enhancements can be seen just above the lowest three harmonics of the proton (H^+) cyclotron frequency. Originally it was thought that these waves were driven by field-aligned currents. However, more recent studies suggest that these waves are produced by ion beams accelerated upward along the auroral field lines by the same quasi-static electric fields that produce the electron precipitation responsible for the aurora. Electrostatic ion cyclotron waves are also sometimes observed near the magnetic equatorial plane. These waves are believed to be driven by energetic ions trapped near the magnetic equator.

Observations of electrostatic ion cyclotron waves in other planetary magnetospheres are very limited. Since the Voyager spacecraft did not pass through the high-latitude auroral regions at the giant planets, with the possible exception of Neptune, no opportunity existed to search for electrostatic ion cyclotron waves driven by auroral processes. Barbosa and Kurth (1990) have interpreted a narrow band of low-frequency waves observed in the cold plasma torus at Jupiter as electrostatic ion cyclotron waves. They suggest that these waves are produced by a charge-exchange interaction between neutral gas emissions from volcanoes on Io and the rapidly rotating Io plasma torus, which is locked to the rotation of Jupiter. This charge-exchange process produces a ring-type ion distribution (sometimes called pick-up ions) and is expected to provide a very effective free energy source for generating electrostatic ion cyclotron waves. Barbosa and Kurth (1990) have also interpreted a band of low-

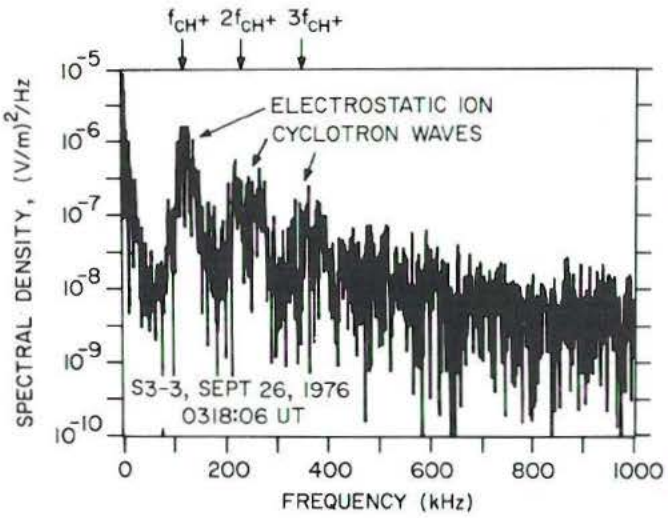

Figure P40 An electric field spectrum of electrostatic ion cyclotron waves observed in the Earth's magnetosphere by the S3–3 spacecraft. These waves occur between harmonics of the proton cyclotron frequency (f_{CH^+}) and are driven by currents flowing along the auroral field lines. (Kintner, Kelley and Mozer, 1978; copyright American Geophysical Union.)

frequency electric field noise in Neptune's magnetosphere as electrostatic ion cyclotron waves, also driven by the same charge-exchange process. Unfortunately, in neither case is it possible to confirm the electrostatic character of the waves, so the identification of the mode is not completely certain.

Electromagnetic ion cyclotron waves

Electromagnetic ion cyclotron waves are very similar to whistler-mode waves, except that they are left-hand polarized and propagate below the ion cyclotron frequency (Table P10). Since the ion cyclotron frequency is much lower than the electron cyclotron frequency [equation (P10)], ion cyclotron waves necessarily occur at extremely low frequencies, typically a few hundred hertz or less. Since the wave field of an electromagnetic ion cyclotron wave rotates in the same sense as positive ions (i.e. left-hand with respect to the magnetic field), these waves interact strongly with positively charged ions. Almost all of the ions observed in planetary magnetospheres are positively charged. The cyclotron resonance condition is identical to equation (P16), except that (e) is replaced by (i). Electromagnetic ion cyclotron waves are driven unstable by a loss cone in the energetic ion distribution. Since a loss cone is always present in a planetary radiation belt, the growth of these waves provides a mechanism for scattering energetic ions into the loss cone, thereby controlling the loss of radiation belt ions.

Despite the intense theoretical interest in the generation of electromagnetic ion cyclotron waves in planetary magnetospheres, relatively few observations are available. The first report of spontaneously generated electromagnetic ion cyclotron waves in the Earth's magnetosphere was by Taylor, Parady and Cahill (1975). These and other subsequent observations (Kintner, Kelley and Mozer, 1977; Roux *et al.*, 1982) have shown that electromagnetic ion cyclotron waves are generated in the Earth's radiation belt during magnetic storms, when intense fluxes of energetic (10 to 100 keV) ions are injected deep into the inner regions of the magnetosphere. Electromagnetic ion cyclotron waves have also been observed at Jupiter by Thorne and Scarf (1984) using Voyager 1 measurements, and by Stone *et al.* (1992) using Ulysses measurements. In both cases intense waves were observed at frequencies below the proton cyclotron frequency. The Ulysses observations are particularly important because the magnetic field of the wave was measured, which confirms that the waves are electromagnetic and not electrostatic (Voyager had only an electric antenna). The ion precipitation produced by these waves is believed to be responsible for the extreme ultraviolet (EUV) aurora at Jupiter (Thorne and Moses, 1983). Using Voyager 2 Neptune data, Gurnett *et al.* (1989) reported observations of a strong band of electric field noise at Neptune at frequencies below the proton cyclotron frequency. This band of electric field noise was tentatively identified as electromagnetic ion cyclotron waves. However, since no wave magnetic field measurements were available, it was not possible to establish definitely the mode of propagation.

Conclusion

This review has described the primary types of plasma waves observed in the vicinity of the planets Venus, Mars, Earth, Jupiter, Saturn, Uranus and Neptune. These observations are summarized in Table P11. By necessity we have not attempted to describe the detailed nature of the observations at each planet. For a more detailed description, see the review by Kurth and Gurnett (1991). In making comparisons between these planets it must be recognized that the observations are in many cases incomplete, particularly at Uranus and Neptune, where the available data are limited to only one pass by the planet. At the giant planets almost no information is available at high magnetic latitudes, a region that we know from terrestrial observations has many complex aurora-related plasma wave emissions. No plasma wave observations have been obained at Mercury and Pluto. Thus there are very significant gaps in our knowledge. It is likely to be many years before these gaps are filled. The most promising missions for future plasma wave investigations are Galileo, which is to orbit Jupiter in late 1995, and Cassini, which is to orbit Saturn early in the 21st century; both spacecraft include plasma wave instruments.

Donald A. Gurnett

Bibliography

Allcock, G. McK. (1957) A study of the audio-frequency radio phenomena known as 'dawn chorus,' *Aust. J. Phys.*, **10**, 286–98.

Barbosa, D.D., and Kurth, W.S. (1990) Theory and observations of electrostatic ion waves in the cold ion torus. *J. Geophys. Res.*, **95**, 6443–50.

Table P11 A summary of the observations of various types of plasma waves at all the planets except Mercury and Pluto

Type of plasma wave	Venus	Earth	Mars	Jupiter	Saturn	Uranus	Neptune
Upstream electron plasma oscillations	×	×	×	×	×	×	×
Upstream ion acoustic waves		×	×	×			
Electrostatic noise at the bow shock	×	×	×	×	×	×	×
Electron cyclotron harmonic waves		×		×	×	×	×
Upper hybrid resonance waves		×		×	×	×	×
Whistler-mode hiss		×		×	×	×	×(?)
Whistler-mode chorus		×		×	×	×	
Whistler-mode auroral hiss		×		×			
Electrostatic ion cyclotron waves		×		×(?)			×(?)
Ion cyclotron whistlers (lightning)		×					
Electromagnetic ion cyclotron emissions		×		×			×(?)

Barkhausen, H. (1919) Zwei mit Hilfe der neuen Verstärker entdeckte Erscheinungen. *Phys. Z.*, **20**, 401.
Barrington, R.E. and Belrose, J.S. (1963) Preliminary results from the very-low frequency receiver aboard Canada's Alouette satellite. *Nature*, **198**, 651–6.
Brice, N. (1964) Fundamentals of very low frequency emission generation mechanisms. *J. Geophys. Res.*, **69**, 4515–22.
Fahleson, U.V. (1967) Theory of electric field measurements conducted in the magnetosphere with electric probes. *Space Sci. Rev.*, **7**, 238–62.
Fredricks, R.W., Kennel, C.F., Scarf, F.L. *et al.* (1968) Detection of electric-field turbulence in the Earth's bow shock. *Phys. Rev. Lett.*, **21**, 1761–4.
Grard, R., Nairn, C., Pedersen, A. *et al.* (1991) Plasma and waves around Mars. *Planet. Space Sci.*, **39**, 89–98.
Gurnett, D.A. (1992) Planetary radio emissions, in *Astronomy and Astrophysics Encyclopedia* (ed. S.P. Maran). New York: Van Nostrand Reinhold, p. 535–7.
Gurnett, D.A. and Frank, L.A. (1978) Ion acoustic waves in the solar wind. *J. Geophys. Res.*, **83**, 58–74.
Gurnett, D.A., Kurth, W.S., Poynter, R.L. *et al.* (1989) First plasma wave observations at Neptune. *Science*, **246**, 1494–8.
Gurnett, D.A., Kurth, W.S., Roux, A. *et al.* (1991) Lightning and plasma wave observations from the Galileo flyby of Venus. *Science*, **253**, 1522–5.
Gurnett, D.A., Kurth, W.S. and Scarf, F.L. (1979a) Plasma wave observations near Jupiter: initial results from Voyager 2. *Science*, **206**, 987–91.
Gurnett, D.A., Kurth, W.S. and Scarf, F.L. (1979b) Auroral hiss observed near the Io plasma torus. *Nature*, **280**, 767–70.
Gurnett, D.A., Kurth, W.S. and Scarf, F.L. (1981) Plasma waves near Saturn: initial results from Voyager 1. *Science*, **212**, 235–9.
Gurnett, D.A., Kurth, W.S., Scarf, F.L. and Poynter, R.L. (1986) First plasma wave observations at Uranus. *Science*, **233**, 106–9.
Gurnett, D.A. and O'Brien, B.J. (1964) High-latitude geophysical studies with satellite Injun 3, 5. Very-low-frequency electromagnetic radiation. *J. Geophys. Res.*, **69**, 65–89.
Gurnett, D.A., and Shaw, R.R. (1973) Electromagnetic radiation trapped in the magnetosphere above the plasma frequency. *J. Geophys. Res.*, **78**, 8136–49.
Gurnett, D.A., Shaw, R.R., Anderson, R.R. *et al.* (1979) Whistlers observed by Voyager 1: Detection of lightning on Jupiter. *Geophys. Res. Lett.*, **6**, 511.
Jones, D. (1980) Latitudinal beaming of planetary radio emissions. *Nature*, **288**, 225–9.
Kennel, C.F., and Petschek, H.E. (1966) Limit on stably trapped particle fluxes. *J. Geophys. Res.*, **71**, 1–28.
Kennel, C.F., Scarf, F.L., Fredricks, R.W. *et al.* (1970) VLF electric field observations in the magnetosphere. *J. Geophys. Res.*, **75**, 6136–52.
Kindel, J.M. and Kennel, C.F. (1971) Topside current instabilities. *J. Geophys. Res.*, **76**, 3055–78.
Kintner, P.M., and Gurnett, D.A. (1977) Observations of ion cyclotron waves within the plasmasphere by Hawkeye 1. *J. Geophys. Res.*, **82**, 2314–8.
Kintner, P.M., Kelley, M.C. and Mozer, F.S. (1978) Electrostatic hydrogen cyclotron waves near one Earth radius altitude in the polar magnetosphere. *Geophys. Res. Lett.*, **5**, 139–42.
Krall, N.A., and Trivelpiece, A.W. (1973) *Principles of Plasma Physics*. New York: McGraw-Hill.
Kurth, W.S. (1991) Continuum radiation in planetary magnetospheres, in *Planetary Radio Emissions III* (eds H.O. Rucker, S.J. Bauer and M.L. Kaiser). Vienna, Austria. Verlage der Osterreichischen Akademie der Wissenschaften, p. 329–50.
Kurth, W.S., and Gurnett, D.A. (1991) Plasma waves in planetary magnetospheres. *J. Geophys. Res.*, **96**, 18877–991.
Melrose, D.B. (1981) A theory for the nonthermal radio continuum in the terrestrial and Jovian magnetospheres. *J. Geophys. Res.*, **86**, 30–6.
Roux, A., Perraut, S. Rauch, J.L. *et al.* (1982) Wave–particle interactions near ω_{He+} observed on board Geos 1 and 2, 2. Generation of ion cyclotron waves and heating of He^+ ions. *J. Geophys. Res.* **87**, 8174–90.
Scarf, F.L., Gurnett, D.A. and Kurth, W.S. (1979) Jupiter plasma wave observations: an initial Voyager 1 overview. *Science*, **204**, 991–5.
Scarf, F.L., Taylor, W.W.L. and Green, I.M. (1979) Plasma waves near Venus: initial observations. *Science*, **203**, 748–50.
Scarf, F.L., Fredricks, R.W., Frank, L.A. and Neugebauer, M. (1971) Nonthermal electrons and high-frequency waves in the upstream solar wind, 1. Observations. *J. Geophys. Res.*, **76**, 5162–71.
Scarf, F.L., Gurnett, D.A., Kurth, W.S. and Poynter, R.L. (1982) Voyager 2 plasma wave observations at Saturn. *Science*, **215**, 587–94.
Scarf, F.L., Fredricks, R.W., Frank, L.A. *et al.* (1970) Direct correlations of large amplitude waves with suprathermal protons in the upstream solar wind. *J. Geophys. Res.*, **75**, 7316–72.
Scudder, J.D., Mangeney, A., Lacome, C. *et al.* (1986) The resolved layer of a collisionless, high β, supercritical, quasi-perpendicular shock wave, 3. Vlasov electrodynamics. *J. Geophys. Res.*, **91**, 11075–97.
Shaw, R.R. and Gurnett, D.A. (1975) Electrostatic noise bands associated with the electron gyrofrequency and plasma frequency in the outer magnetosphere. *J. Geophys. Res.*, **80**, 4259–71.
Stix, T. (1962) *The Theory of Plasma Waves*. New York: McGraw-Hill, 110 pp.
Stone, R.G., Pedersen, B.M., Harvey, C.C. *et al.* (1992) Ulysses radio and plasma wave observations in the Jupiter environment. *Science*, **257**, 1524–30.
Storey, L.R.O. (1953) An investigation of whistling atmospherics. *Phil. Trans. Roy. Soc. London*, A, **46**, 113–41.
Taylor, W.W.L., Parady, B.K. and Cahill, L.J. Jr, (1975) Explorer 45 observations of 1- to 30-Hz magnetic fields during magnetic storms. *J. Geophys. Res.*, **80**, 1271–86.
Thorne, R.M. and Moses, J. (1983) Electromagnetic ion-cyclotron instability in the multi-ion Jovian magnetosphere. *Geophys. Res. Lett.*, **10**, 631–4.
Thorne, R.M., and Scarf, F.L. (1984) Voyager 1 evidence for ion-cyclotron instability in the vicinity of the Io plasma torus, *Geophys. Res. Lett.*, **11**, 263–6.

Acknowledgement

This research was supported by NASA through contract 959193 with the Jet Propulsion Laboratory.

Cross references

Heliosphere
Magnetospheres of the outer planets
Planetary torus
Shock waves
Solar wind
Thermal plasma instrumentation
Voyager missions
Whistler

PLATE TECTONICS

The Earth's solid surface behaves in most places as if it were divided into a number of almost rigid 'plates'. Any horizontal motion of a rigid plate on a spherical Earth is necessarily a rotation about an axis through the center. This axis cuts the surface at the 'pole of rotation'. The plates move relative to one another over the asthenosphere (q.v.) at speeds of the order of 10–100 mm per year. Two good modern textbooks on the subject are Cox and Hart (1986) and Fowler (1990).

Figure P41 is a map of shallow earthquakes, which mark the plate boundaries well in the oceans but less so in continental areas. At mid-ocean ridges (Figure P42) the ocean is typically 2.5 km shallower than average; the plates are moving apart; hot, soft asthenosphere rises and turns into hard, cold sea floor; and there are only shallow earthquakes. The opposite sides of oceanic plates usually have 'subduction zones' where the plates bend and go down into the mantle. These zones are marked by trenches several kilometers deeper than normal ocean nearby; by earthquakes which are shallow near the trenches, and become deeper with distance away from them; and by lines of andesitic volcanoes above the earthquakes 100–200 km deep.

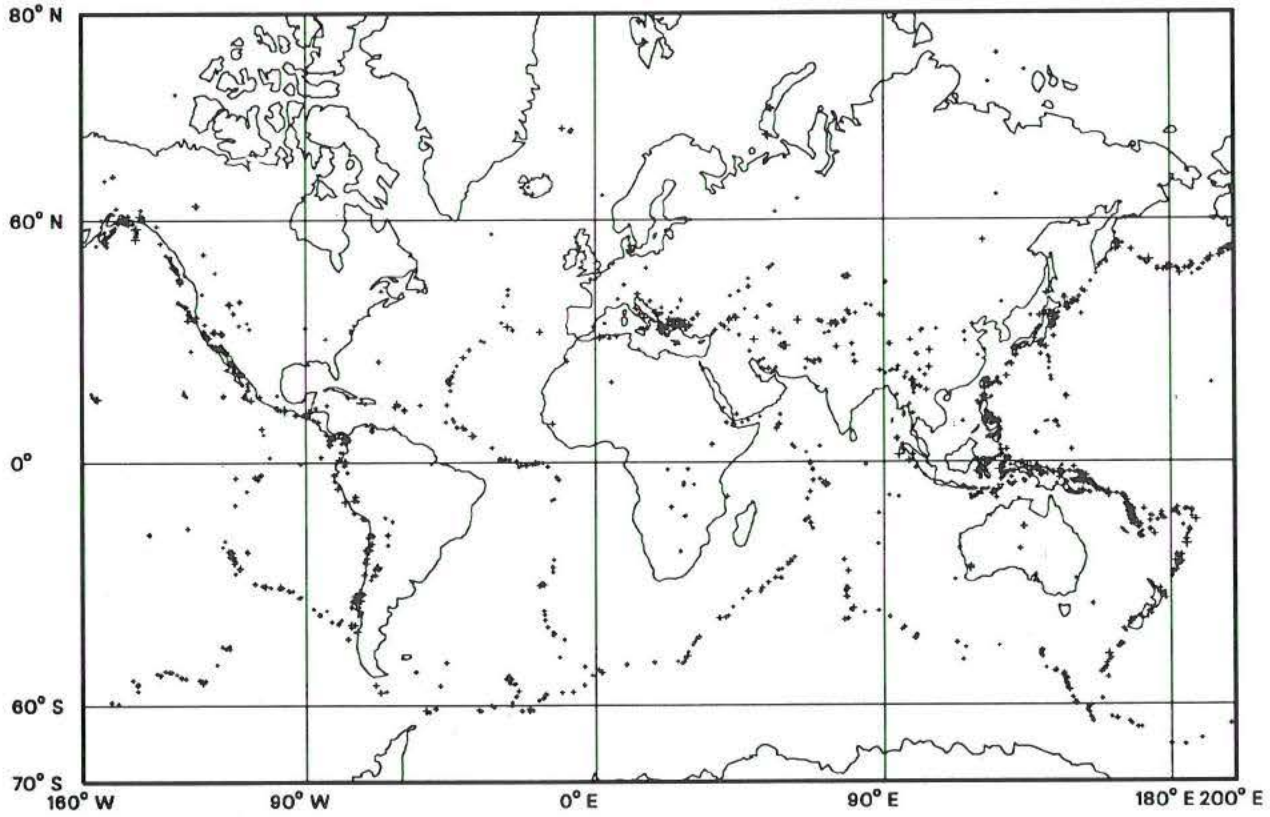

Figure P41 Earthquakes over magnitude 5.5 and shallower than 20 km, from the USGS Global Hypocenter Data Base. Larger + marks indicate larger earthquakes.

Continental plate collision zones are marked in the same way as subduction zones in Figure P42; the difference is that ocean plates subduct, to depths of at least several hundred kilometers, whereas continental plates do not. They normally pile up in a mountain range instead; the largest example is the Himalayas. At transform faults, the remaining type of plate boundary, one plate slides horizontally past the other, with little or no rising or sinking of crustal material.

All plate boundaries are seismically active: subduction zones the most, transform faults less so (there may even be continuously creeping segments with no earthquakes, as in parts of the San Andreas fault in California), and ridges least of all.

Figure P43 is a schematic, true-scale cross-section of a typical region of the Earth, showing a subduction zone, a ridge and parts of three plates. On this scale oceans and mountains are invisible, and only the most violent volcanic eruptions throw ash high enough to be seen.

No two experts in the field would be likely to show exactly the same map of the plates. For example, DeMets *et al.* (1990) separate the Indian and Australian plates along a nearly east–west line between the Carlsberg and Central Indian ridges, and do not show the Scotia or Sandwich plates as separate from the Antarctic. (The Sandwich plate is the small D-shaped area just east of the Scotia plate in Figure P42.) Other authors show more 'microplates', e.g., separating an Adriatic plate from the African and Eurasian plates (Anderson, 1987), or the Caroline basin from the Pacific plate (Weissel and Anderson, 1978), or inserting Easter and Juan Fernandez microplates on the Nazca–Pacific plate boundary (Hey *et al.*, 1985). The location of both dashed boundaries in Figure P42 is controversial.

In continental regions being compressed by plate motion, the deformation may be so widespread that it is doubtful whether the concept of plate behavior is useful at all. Molnar and Tapponnier (1975) suggested that the eastward motion of Tibet and nearby areas is better explained in terms of plastic flow throughout the region, as India continues to be pushed north into it. For people trying to understand the Earth as a whole, plate tectonics is a useful large-scale model. Even for those concentrating on a deforming region like Tibet or New Zealand, plate tectonics provides at least the boundary conditions at a large distance, and helps to explain why the deformation occurs.

History

Plate tectonics appeared during the 1960s as a synthesis of much previous work. The history is well described by Cox (1973) and Emiliani (1981). References for this section not listed below can be found in one or other of those books. Both show the subject as a fine example of how major changes occur in scientific understanding.

The general idea of currents inside the Earth leading to surface displacements dates back to the 19th century. In the early 20th century Wegener introduced the concept of drifting continents, which neatly explained a variety of topographic, sedimentological, paleontological, botanical and zoological observations. Wegener had no convincing driving mechanism, however, and so failed to convince many people (except in the southern hemisphere, where the field evidence for former connections of continents now separated was much stronger than in the northern hemisphere).

Hills (1934) drew the analogy between froth floating on boiling jam and moving continents floating on the mantle of the Earth, in each case the driving mechanism being thermal convection. Jeffreys (1934) admitted that this sort of driving mechanism would avoid his earlier objection (on mechanical grounds) to continents ploughing their way across basaltic ocean floors. Both authors thought that such movements had stopped early in the history of the Earth.

The seismological results of Gutenberg and Richter (1949) did not immediately lead to the emergence of plate tectonics, in spite of their maps which were very like Figures P41 and P42, mainly because oceanic geology was too little known at the time. Neither did the work of Runcorn in 1962 on paleomagnetism (q.v.). He and many others deduced polar wander paths from observations of the direction (in three dimensions) in which dated rocks in different parts of the world are found to be magnetized. From land-based paleomagnetic work the major conclusion was that about 200 million years ago the